CUL-2^{LRR-1} and UBXN-3 drive replisome disassembly during DNA replication termination and mitosis

Sonnerville, Remi; Priego Moreno, Sara; Knebel, Axel; Johnson, Clare; Hastle, C. James; Gartner, Anton; Gambus, Agnieszka; Labib, Karim

DOI:
10.1038/ncb3500

CUL-2^{LRR-1} and UBXN-3/FAF1 drive replisome disassembly during DNA replication termination and mitosis

Remi Sonneville[1], Sara Priego Moreno[2], Axel Knebel[1], Clare Johnson[1], C. James Hastie[1], Anton Gartner[3], Agnieszka Gambus[2] and Karim Labib[1]

[1]MRC Protein Phosphorylation and Ubiquitylation Unit, School of Life Sciences, University of Dundee, Dow Street, Dundee, DD1 5EH, U.K.

[2]Institute of Cancer and Genomic Sciences, College of Medical and Dental Sciences, University of Birmingham, Edgbaston, Birmingham, B15 2TT, U.K.

[3]Centre for Gene Regulation and Expression, School of Life Sciences, University of Dundee, Dow Street, Dundee, DD1 5EH, U.K.

Correspondence should be addressed to a.gambus@bham.ac.uk or kpmlabib@dundee.ac.uk.

Abstract

Replisome disassembly is the final step of DNA replication in eukaryotes, involving the ubiquitylation and CDC48-dependent dissolution of the CMG helicase (Cdc45-MCM-GINS). Using *Caenorhabditis elegans* early embryos and *Xenopus* egg extracts, we show that the E3 ligase CUL-2^{LRR-1} associates with the replisome and drives ubiquitylation and disassembly of CMG, together with the CDC-48 co-factors UFD-1 and NPL-4. Removal of CMG from chromatin in frog egg extracts requires CUL2 neddylation, and our data identify chromatin recruitment of CUL2^{LRR1} as a key regulated step during DNA replication termination. Interestingly, however, CMG persists on chromatin until prophase in worms that lack CUL-2^{LRR-1}, but is then removed by a mitotic pathway that requires the CDC-48 co-factor UBXN-3, orthologous to the human tumour suppressor FAF1. Partial inactivation of *lrr-1* and *ubxn-3* leads to synthetic lethality, suggesting future approaches by which a deeper understanding of CMG disassembly in metazoa could be exploited therapeutically.

Keywords: DNA replication termination; replisome disassembly; CMG helicase; *Caenorhabditis elegans*; *Xenopus laevis*; Cullin; CUL-2; LRR-1; UBXN-3; FAF1; CUL2; LRR1; CDC-48, UFD-1; NPL-4; p97; VCP; ULP-4

Chromosome replication in eukaryotes is initiated by the assembly of the CMG helicase at origins of DNA replication[1, 2]. CMG then controls the progression of DNA replication forks, by unwinding the parental DNA duplex to form the single-strand substrate for DNA polymerases[3, 4]. The CMG helicase forms the core of the eukaryotic replisome[1, 5] and must remain associated with replication forks throughout elongation, since it cannot be reloaded[6]. The catalytic core of the helicase is formed by a hexameric ring of the MCM2-7 proteins, which is topologically trapped around the DNA template and is stabilised and activated by association with CDC45 and GINS[1, 7].

The remarkably stable association of CMG with replication forks means that a specialized mechanism is needed to remove the helicase and trigger replisome disassembly during DNA replication termination[8]. In budding yeast and *Xenopus* egg extracts, the CMG helicase was found to be ubiquitylated on its Mcm7 subunit in a late step of DNA replication[9-11], leading rapidly to a disassembly reaction that requires the CDC48/p97 AAA+ ATPase[10, 11].

In *Saccharomyces cerevisiae*, the cullin 1-based E3 ligase SCF^{Dia2} associates with the replisome and is essential for CMG ubiquitylation and disassembly[10, 12, 13]. Orthologues of the F-box protein Dia2 are not apparent in metazoa, but a putative role for a metazoan cullin ligase during DNA replication termination was suggested by the fact that CMG ubiquitylation and disassembly are inhibited in *Xenopus* egg extracts[11] by the neddlylation inhibitor MLN4924[14], since the major role of neddylation is to activate cullin ligases[15, 16].

Here we describe a screen for factors controlling CMG helicase disassembly in the *C. elegans* early embryo, leading to the identification of a cullin ligase that we show is also essential for chromatin extraction of CMG during S-phase in *Xenopus* egg extracts, where we find that recruitment of the ligase to chromatin is a key regulated step during DNA replication termination. We also identify a second pathway for CMG helicase disassembly during mitosis in *C. elegans*, indicating that replisome disassembly in metazoa involves additional mechanisms not previously identified in yeast.

Results

A cytological assay for replisome dissolution in *C. elegans* early embryos

We established an *in vivo* assay for defects in replisome disassembly in live *C. elegans* early embryos (Figure 1), by time-lapse analysis of embryos simultaneously expressing mCherry-Histone H2B and GFP-tagged CMG components[17, 18]. We initially examined GFP-tagged versions of CDC-45 and the GINS component SLD-5, after depletion of CDC-48. As shown in Supplementary Figure 1a, both GFP-CDC-45 and GFP-SLD-5 were absent from chromatin during prophase in control embryos, but were chromatin-associated throughout mitosis in embryos treated with *cdc-48* RNAi. We also screened all the known or predicted adaptors of worm CDC-48[19-21] (Supplementary Figure 1b), and found that depletion of either subunit of the NPL-4_UFD-1 heterodimer[22, 23] led to persistence of both GINS and CDC-45 on condensing prophase chromatin (Figure 1b-c, Supplementary Figure 1c, Supplementary Movies 1-2). Moreover, a fraction of GFP-MCM-3 was

present on chromatin during early mitosis in embryos depleted for NPL-4 or CDC-48 (Figure 1d and Supplementary Figure 1d-e, *npl-4* or *cdc-48* RNAi, 'early metaphase'; note that the high concentration of MCM-2-7 in the nucleus precluded the examination of prophase chromatin). Finally, we used fluorescence recovery after photobleaching (FRAP) to confirm that *npl-4* RNAi caused 'old' CMG components to persist on chromatin after S-phase, rather than driving the premature assembly of 'new' CMG complexes (Figure 1h, Supplementary Movie 3, Supplementary Figure 1g-h). These findings indicated that CDC-48 and its co-factors NPL-4 and UFD-1 are essential for the extraction of CMG components from chromatin during S-phase in the *C. elegans* early embryo.

Consistent with these data, we found that *npl-4* RNAi led to a strong accumulation of the CMG helicase with ubiquitylated MCM-7 subunit (Figure 1e-g). Ubiquitylation of CMG was reduced if the completion of DNA replication was inhibited (Supplementary Figure 1f), by RNAi depletion of the ribonucleotide reductase RNR-1 as described previously[18], consistent with the idea that CMG ubiquitylation in the worm embryo is linked to DNA replication termination as in budding yeast and *Xenopus laevis*[10, 11].

CUL-2^{LRR-1} is required for ubiquitylation and disassembly of the CMG helicase during S-phase in *C. elegans*

The *C. elegans* genome encodes CUL-1 to CUL-5 (Supplementary Figure 2a), which are orthologues of the five cullins found in diverse metazoa, plus CUL-6 that is a paralogue of CUL-1[24]. Using our cytological assay for

CMG disassembly, we found that RNAi depletion of CUL-2 was unique in causing persistence of SLD-5 and PSF-1 on prophase chromatin (Figure 2a, Supplementary Figure 2b and Supplementary Movie 4). The same defect was observed after depletion of the RING finger protein Rbx1, which links CUL-2 (and CUL-1/3/4/6) to its cognate ubiquitin conjugating enzyme, or after depletion of the worm orthologues of Elongin B and Elongin C, which connect CUL-2 (and CUL-5) to its substrate adaptors (Figure2a; see below for Elongin B). These findings indicated that a CUL-2 ligase regulates disassembly of the CMG helicase during S-phase in *C. elegans*, probably involving ubiquitin ligase activity, since not only CUL-2 but also RBX-1 is required for removing CMG from chromatin.

Six different substrate adaptors of CUL-2 have been characterized in *C. elegans* (Supplementary Figure 2c), five of which are conserved in humans. We depleted each of these and found that RNAi to *lrr-1* (Leucine-rich repeats 1) was unique in causing GINS and CDC-45 to persist on prophase chromatin (Figure 2b, Supplementary Figure 2d and Supplementary Movie 5 for GINS; see Supplementary Figure 3d below for CDC-45). Importantly, depletion of LRR-1 also dramatically reduced CMG ubiquitylation, when replisome disassembly was blocked by *npl-4* RNAi (Figure 2c-d). These data indicated that CUL-2^{LRR-1} regulates CMG disassembly during DNA replication termination in the *C. elegans* early embryo.

A mitotic pathway for CMG chromatin extraction requires the CDC-48 co-factor UBXN-3

Although CMG was initially retained on prophase chromatin following RNAi depletion of CUL-2^{LRR-1}, both GINS and CDC-45 were then released from chromatin a few minutes before nuclear envelope breakdown in late prophase (Figure 3a, Supplementary Figure 3a, b, d, and Supplementary Movies 4-5; note that MCM-2-7 could not be examined on prophase chromatin, as discussed above). Moreover, the same was true in *lrr-1Δ* / *lrr-1Δ* homozygous embryos that lack the LRR-1 protein (Figure 3c and Supplementary Figure 3c; *lrr-1* is an essential gene in *C. elegans*, but the first embryonic cell cycles in homozygous *lrr-1Δ* embryos can be examined as described in Methods). The delayed release of CMG components from chromatin in the absence of LRR-1 was not produced by a delay in the completion of S-phase, since RNAi depletion of the catalytic or primase subunits of Pol alpha greatly extended the length of S-phase, yet did not cause CMG to persist on condensing chromatin (Figure 3a-b, *div-1* and *pol alpha* RNAi), consistent with our previous data[17]. Instead, these findings indicated that the *C. elegans* early embryo has two different pathways for CMG helicase disassembly (Supplementary Figure 3e). The first pathway acts during DNA replication termination and requires CUL-2^{LRR-1}, whereas the second provides backup and is activated during prophase. Consistent with the existence of the second pathway, we found that depletion of LRR-1 did not cause a strong accumulation of CMG in embryo extracts, compared to depletion of NPL-4 (Figure 3d, compare samples 2 and 3). However, *lrr-1* RNAi did abrogate the basal level of CMG ubiquitylation that is seen in control embryos (Figure 3d-e, longer exposures, compare samples 1 and 2).

Both CMG disassembly pathways require CDC-48 / UFD-1 / NPL-4, since depletion of the latter leads to persistence of CMG on chromatin throughout mitosis (Figure 1, Supplementary Figure 1). In addition to the three 'core' co-factors that form mutually exclusive complexes with CDC-48 / p97, namely UFD-1_NPL-4, UBXN-2 / p47 and UBXN-6 / UBXD1, eukaryotic cells also contain a range of other partners of p97 / CDC-48 that recruit the segregase to specific targets or to particular sub-cellular locations[25-27] (Supplementary Figure 1b). To test whether one of these links CDC-48 to the mitotic CMG disassembly pathway, we combined *lrr-1* RNAi with depletion of each of the predicted CDC-48 adaptors in *C. elegans* (see Methods), and then examined the association of CMG components with mitotic chromatin. Amongst all the tested combinations, only simultaneous depletion of LRR-1 and UBXN-3 led to persistence of GFP-CDC-45, GFP-PSF-1 and GFP-SLD-5 on mitotic chromatin (Figure 4a, Supplementary Figure 4a-b and Supplementary Movie 6). In contrast, these CMG components were released from chromatin before prophase in embryos treated with RNAi to *ubxn-3* alone (Figure 4a, Supplementary Figure 4a-b and Supplementary Movie 7).

To assay directly the level of the CMG helicase in the presence or absence of UBXN-3, we isolated GFP-PSF-1 from embryo extracts as above. Simultaneous RNAi to *ubxn-3* and *lrr-1* led to a striking accumulation of CMG, equivalent to that seen with *npl-4* RNAi (Figure 4b, compare level of CDC-45 and MCM-2 associated with GINS in samples 2-4), with residual ubiquitylation of CMG as seen with *npl-4 lrr-1* RNAi (compare Figure 4b samples 3-4 with Figure 3d-e samples 3-4). Together with the imaging data described above,

these findings identify UBXN-3 as a factor required for a mitotic pathway of CMG disassembly in the *C. elegans* early embryo.

The SUMO protease ULP-4 modulates the mitotic CMG disassembly pathway

To screen for regulators of the mitotic CMG disassembly pathway, we combined *lrr-1* RNAi with depletion of candidate proteins, including factors that regulate cell division or genome integrity (Supplementary Table 1). These included mitotic regulators such as the Aurora B and Polo kinases AIR-2 and PLK-1, candidate ubiquitin ligases such as BRC-1 (BRCA1) and SMC-5, regulators of DNA replication such as the ATL-1 checkpoint kinase, and components of the SUMO pathway. Uniquely amongst these factors, we found that co-depletion of the SUMO protease ULP-4 with LRR-1 delayed the release of CMG components from chromatin, until at or after nuclear envelope breakdown, (Figure 4c and Supplementary Figure 4c-d). ULP-4 is the major SUMO protease during mitosis in *C. elegans*, analogous to SENP6-7 in human cells, and is present on mitotic chromosomes and at the spindle midzone [28]. Although *ulp-4 lrr-1* RNAi produced a less severe CMG disassembly defect than co-depletion of LRR-1 and UBXN-3, these findings indicated that the UBXN-3-dependent mitotic pathway for CMG disassembly is also modulated by ULP-4.

Combining defects in the S-phase and mitotic CMG disassembly pathways produces synthetic lethality

Previous work showed that LRR-1 is essential for germ cell formation and embryonic development in *C. elegans*[29, 30]. In contrast, RNAi to *ubxn-3* or *ulp-4* is tolerated without causing severe embryonic lethality (see below), indicating that the mitotic CMG disassembly pathway is dispensable in worms that can disassemble CMG via the CUL-2^{LRR-1} S-phase pathway.

To explore the physiological importance of the mitotic CMG disassembly pathway should CUL-2^{LRR-1} fail to act, we fed worms on bacteria with 10% expressing *lrr-1* RNAi (Figure 4d shows that this low dose of lrr-1 RNAi scarcely affects viability), and then gradually increased the proportion of bacteria that expressed RNAi to *ubxn-3* or *ulp-4*. Strikingly, even the lowest tested dose of *ubxn-3* RNAi produced 100% lethality in combination with 10% *lrr-1* RNAi, despite both single RNAi treatments causing almost no detectable lethality (Figure 4e). Similarly, the lowest tested dose of *ulp-4* RNAi produced 90% embryonic lethality in combination with 10% *lrr-1* RNAi, even though neither individual RNAi treatment affected viability to a significant degree (Figure 4f). These findings indicate that both UBXN-3 and ULP-4 become essential when the function of CUL-2^{LRR-1} is even partially defective, consistent with the possibility that the mitotic CMG disassembly pathway provides an essential back up for the S-phase pathway (though this remains to be demonstrated directly in future studies).

LRR-1 couples the CUL-2^{LRR-1} ubiquitin ligase to the worm replisome

To test whether CUL-2^{LRR-1} associates with the worm replisome, we treated control and *GFP-psf-1* worms with *npl-4* RNAi to block replisome

disassembly, and then used isolated embryos to generate extracts that were incubated with beads coupled to anti-GFP antibodies. A fraction of the resultant material was analysed by immunoblotting, to confirm the specific isolation of ubiquitylated CMG helicase from the *GFP-psf-1* embryos (Figure 5a). The remainder was resolved by SDS-PAGE (Figure 5b) and analysed by mass spectrometry (Supplementary Table 2).

The worm CMG helicase and associated factors showed remarkable convergence with the better-characterized replisome from budding yeast (Supplementary Table 2, Figure 5c: note that our data represent the worm replisome just after termination of DNA synthesis). Notably, CUL-2^{LRR-1} was the only cullin ligase associated with the post-termination worm replisome (Supplementary Table 2), and we subsequently found that the presence of CUL-2 in the purified material was dependent upon LRR-1 (Figure 5d, Supplementary Table 3). Therefore, LRR-1 is required for CUL-2 to associate with the replisome in *C. elegans* early embryos.

CUL2^{LRR1} associates with the vertebrate replisome during DNA replication termination in *Xenopus* egg extracts

In analogous experiments, we examined whether CUL2^{LRR1} associated with the vertebrate replisome during DNA replication termination in *Xenopus* egg extracts. Sperm nuclei were added to an extract supplemented with a dominant negative p97 mutant as well as the neddylation inhibitor MLN4924, both of which block CMG disassembly at the end of S-phase[11]. After bulk DNA replication had been completed (see below), the CMG helicase was

isolated from the chromatin fraction by DNA digestion followed by immunoprecipitation of MCM3 (Figure 6a; non-specific IgG was used as a negative control). The resultant material was then analysed by mass spectrometry and found to contain orthologues of every component of the isolated post-termination worm replisome (Supplementary Table 4). Strikingly, the post-termination vertebrate replisome was associated with a single cullin ligase, namely $CUL2^{LRR1}$ (Supplementary Table 4, Figure 6b). Correspondingly, immunoprecipitation of LRR1 from digested chromatin, after inhibition of replisome disassembly with a p97 inhibitor, led to co-purification not only of CUL2 and Elongin B/C, but also of the frog replisome (Figure 6c, Supplementary Table 5). Interestingly, immunoprecipitation of LRR1 from digested chromatin under such conditions led to co-depletion of CUL2 (Supplementary Figure 5a, compare flowthrough for IgG and LRR1 IPs). Therefore, these data not only demonstrate that the association of $CUL2^{LRR1}$ with the replisome is conserved from worms to vertebrates, but also indicate that $CUL2^{LRR1}$ is the major CUL2 ligase on interphase chromatin.

The recruitment of *Xenopus* $CUL2^{LRR1}$ to chromatin was dependent upon replisome assembly during the initiation of chromosome replication (Figure 6d). Moreover, the association of $CUL2^{LRR1}$ with chromatin was greatly increased when replisome disassembly at the end of S-phase was blocked by addition of MLN4924 to the extracts (Figure 6e: Figure 6f and Supplementary Figure 5b show that replication kinetics were not affected by MLN4924, consistent with our previous findings[11]). These data suggested that regulated recruitment of $CUL2^{LRR1}$ to chromatin is an important feature of

the mechanism of replisome disassembly during DNA replication termination. Correspondingly, $CUL2^{LRR1}$ was not recruited to chromatin if DNA synthesis and subsequent termination were blocked, by addition of the DNA polymerase inhibitor aphidicolin (Figure 6g; note that caffeine had to be added to these reactions, to prevent the S-phase checkpoint pathway from limiting the accumulation of CMG on chromatin, by blocking new initiation events).

To test directly whether chromatin recruitment of $CUL2^{LRR1}$ was linked to DNA replication termination, we either inhibited replisome disassembly after termination of DNA synthesis, by inactivating CDC48 / p97 with the small molecule inhibitor NMS873[31, 32], or delayed the convergence of DNA replication forks during termination, by addition of the TOPO2 inhibitor ICRF193[11, 33]. Neither treatment affected the kinetics of bulk DNA synthesis (Supplementary Figure 5c), consistent with previous studies[9, 11]. Inhibition of p97 / CDC48 with NMS873 caused a dramatic accumulation of CMG and $CUL2^{LRR1}$ on chromatin (Figure 6h, NMS873). However, delaying DNA replication fork convergence with ICRF193 delayed removal of CMG components from chromatin (Figure 6h, compare CDC45 and PSF2 between control and ICRF193 treatment), but this was not associated with chromatin recruitment of $CUL2^{LRR1}$ (Figure 6h). These findings indicate that $CUL2^{LRR1}$ only associates with the replisome during the termination of DNA replication.

Active $CUL2^{LRR1}$ is essential for extraction of the CMG helicase from chromatin at the end of chromosome replication in *Xenopus* egg extracts

Depletion of frog egg extracts with antibodies to CUL2-RBX1 (Figure 7a) abolished detectable chromatin recruitment of $CUL2^{LRR1}$ during DNA replication termination (Figure 7b), even in the presence of MLN4924 that stabilises the association of the ligase with the post-termination replisome as shown above. The kinetics of bulk DNA replication in egg extracts were not affected by CUL2 depletion (Figure 7d-e), but the release of CMG components from chromatin at the end of replication was inhibited (Figure 7f). Moreover, ubiquitylation of the MCM7 subunit of CMG was both delayed and greatly reduced under such conditions (Figure 7f, MCM7).

To confirm that the failure of CMG chromatin extraction was indeed due to inactivation of CUL2-RBX1, we attempted to rescue the defect by addition of recombinant CUL2-RBX1, purified from insect cells. However, we noted that LRR1 was co-depleted from extracts along with CUL2 (Figure 7c), and thus we performed the rescue experiments in the presence or absence of recombinant LRR1, expressed and purified from *E. coli*. By isolating sperm chromatin from *Xenopus* egg extracts after the completion of bulk DNA replication, we confirmed that CMG components were absent from chromatin in mock-depleted extracts that were subjected to two rounds of immunoprecipitation with rabbit IgG (Figure 7g, lane 1), whereas CMG remained on chromatin following depletion of $CUL2^{LRR1}$ (Figure 7g, lane 2), as shown above (Figure 7f). Crucially, the defect in CMG helicase disassembly was not rescued by addition of CUL2-RBX1 complex alone (Figure 7g, lane 3), but was fully complemented by the addition of CUL2-RBX1 together with recombinant LRR1 (Figure 7g, lane 5).

To explore whether the E3 ligase activity of $CUL2^{LRR1}$ was required for CMG chromatin extraction, we tested a version of CUL2-RBX1 with a mutated neddylation site and another mutation in the interaction site with the DCN1 neddylase[34], since neddylation promotes cullin function in vertebrates and we previously showed that the neddylation inhibitor MLN4924 blocks CMG ubiquitylation and chromatin extraction during DNA replication termination in *Xenopus* egg extracts[11]. Importantly, mutated CUL2-RBX1 was not able to restore CMG chromatin extraction in CUL2-depleted extracts (Figure 7g, lane 4), even when added with recombinant LRR1 (Figure 7g, lane 6).

These findings demonstrate that CMG helicase disassembly at the end of chromosome replication in *Xenopus* egg extracts requires LRR1 and neddylation of CUL2, indicating a requirement for active $CUL2^{LRR1}$. Together with past work establishing CMG helicase disassembly as the final regulated step during chromosome replication in vertebrates[9], these findings establish the ubiquitin ligase $CUL2^{LRR1}$ as the key enzyme in this process.

Discussion

Previous work showed that LRR-1 is essential for germ cell formation and embryonic development in *C. elegans*[29, 30]. Inactivation of *lrr-1* induces DNA damage, thereby blocking germ cell proliferation and delaying mitotic entry in the early embryo[29], via the ATL-1 S-phase checkpoint pathway that is equivalent to the ATR response in vertebrates. The molecular basis for DNA damage induction in the absence of LRR-1 is poorly understood, but a recent study found that low-dose RNAi to CMG components could suppress the

sterility phenotype of *lrr-1Δ* worms, as well as suppressing the embryonic lethality associated with a *cul-2* temperature sensitive allele under semi-restrictive conditions[35]. These findings suggest that the CMG helicase is a functionally important target of CUL-2^{LRR-1} in *C. elegans*.

Our data indicate that CUL2^{LRR1} activity is required to extract CMG from chromatin during DNA replication termination, both in worms and in frog egg extracts, indicating that the role of CUL2^{LRR1} in the S-phase pathway of CMG helicase disassembly is widely conserved in metazoa. Moreover, our data identify chromatin recruitment of CUL2^{LRR1} as a key regulated step (Figure 6). We note that a recent study of plasmid replication in *Xenopus* egg extracts has also shown that CUL2^{LRR1} is recruited during termination and is required for replisome disassembly[36], consistent with our findings.

Despite metazoa and yeast using different cullin ligases to trigger replisome disassembly during termination of replication, our data highlight invariant features of the disassembly mechanism in diverse eukaryotes. Firstly, the CMG helicase is ubiquitylated on its MCM7 subunit at the end of chromosome replication in budding yeast[10], worm (this study) and frog[9, 11], perhaps linked to a structural change in the CMG helicase that renders it accessible to the E3 ligase during DNA replication termination. Secondly, we found that UFD-1 and NPL-4 are required for CDC-48-dependent disassembly of the CMG helicase during S-phase in *C. elegans* (Figure 1 and Supplementary 1), and UFD1-NPL4 associate with the 'post-termination' replisome in *Xenopus* (Supplementary Table 4), consistent with previous data[37]. These findings indicate that UFD1 and NPL4 mediate CDC48-

dependent replisome disassembly in metazoa, and we predict that the same is true for budding yeast.

Whereas budding yeast appears to have a single pathway for CMG helicase disassembly that acts during S-phase[10], our *C. elegans* data indicate that metazoa have an additional CMG disassembly mechanism that operates during mitosis and requires the UBXN-3 partner of CDC-48. Interestingly, a recent study found that depletion of UBXN-3 sensitises worm embryos to DNA replication inhibitors, consistent with a role for UBXN-3 in regulation of the replisome[38]. It remains to be determined in future studies whether the mitotic pathway is also controlled by an E3 ubiquitin ligase, analogous to the role of CUL-2^{LRR-1} during S-phase, but we have found that the mitotic CMG disassembly pathway is modulated by the ULP-4 SUMO protease, which is the major desumoylase on mitotic chromosomes[28]. It will thus be interesting to explore whether SUMO regulates CMG helicase disassembly during mitosis, perhaps inhibiting disassembly until desumoyation by ULP-4, or whether ULP-4 acts in some other way, for example by recruiting CDC-48 partners like UBXN-3 to mitotic chromatin.

We have found that UBXN-3 and ULP-4 become essential for viability when the function of LRR-1 is even partially compromised (Figure 4), highlighting the physiological importance of UBXN-3 and ULP-4. These findings suggest that the mitotic CMG disassembly pathway provides important backup to the DNA replication termination pathway, although at present we cannot exclude that our data also reflect other roles for LRR-1, UBXN-3 and ULP-4. Interestingly, the human FAF1 protein is orthologous to

UBXN-3, associates with p97-UFD1-NPL4[39] and is deleted or depleted in many human cancers[40]. Moreover, depletion of FAF1 in human cells leads to defective progression and increased stalling of DNA replication forks[38]. Should it be possible in the future to develop small molecule inhibitors of $CUL2^{LRR1}$, our data indicate that transient or partial inhibition of the $CUL2^{LRR1}$ E3 ligase might cause synthetic lethality in cancer cells with defective FAF1. It is thus to be hoped that a deeper understanding of the biology of replisome disassembly during DNA replication termination will have important implications for human pathology.

Acknowledgements

We gratefully acknowledge the support of the Medical Research Council (core grant MC_UU_12016/13 for KL; award MR/K007106/1 to Agnieszka Gambus) the Wellcome Trust (reference 102943/Z/13/Z for award to KL; reference 0909444/Z/09/Z for award to Anton Gartner) and the Lister Institute (award to Agnieszka Gambus) for funding our work. We thank Julian Blow for Geminin protein, MRC PPU reagents (https://mrcppureagents.dundee.ac.uk) for recombinant frog LRR1 and for producing antibodies, and Tom Deegan for helpful comments on the manuscript. We also thank Lionel Pintard for providing the worm line heterozygous for *lrr-1Δ*, Chris Ponting for advice regarding orthologues of the budding yeast Dia2 protein and Johannes Walter and Emily Low for discussing unpublished findings.

Author Contributions

RS performed the experiments in Figures 1-5 and Figures S1-S4. SPM performed the experiments in Figures 6-7 and Figures S5. KL and Agnieszka Gambus conceived the project and designed experiments in collaboration with RS and SPM. AK and CJ produced recombinant CUL2-RBX1 and JH provided recombinant LRR1. Anton Gartner provided invaluable support in the early stages of the project. KL wrote the manuscript, with contributions and critical comments from the other authors.

References

1. Gambus, A. *et al.* GINS maintains association of Cdc45 with MCM in replisome progression complexes at eukaryotic DNA replication forks. *Nat Cell Biol* **8**, 358-366 (2006).
2. Moyer, S.E., Lewis, P.W. & Botchan, M.R. Isolation of the Cdc45/Mcm2-7/GINS (CMG) complex, a candidate for the eukaryotic DNA replication fork helicase. *Proc Natl Acad Sci U S A* (2006).
3. Bell, S.P. & Labib, K. Chromosome Duplication in Saccharomyces cerevisiae. *Genetics* **203**, 1027-1067 (2016).
4. Deegan, T.D. & Diffley, J.F. MCM: one ring to rule them all. *Curr Opin Struct Biol* **37**, 145-151 (2016).
5. O'Donnell, M. & Li, H. The Eukaryotic Replisome Goes Under the Microscope. *Curr Biol* **26**, R247-256 (2016).

6. Labib, K., Tercero, J.A. & Diffley, J.F.X. Uninterrupted MCM2-7 function required for DNA replication fork progression. *Science* **288**, 1643-1647 (2000).
7. Ilves, I., Petojevic, T., Pesavento, J.J. & Botchan, M.R. Activation of the MCM2-7 helicase by association with Cdc45 and GINS proteins. *Molecular cell* **37**, 247-258 (2010).
8. Bell, S.P. DNA Replication. Terminating the replisome. *Science* **346**, 418-419 (2014).
9. Dewar, J.M., Budzowska, M. & Walter, J.C. The mechanism of DNA replication termination in vertebrates. *Nature* **525**, 345-350 (2015).
10. Maric, M., Maculins, T., De Piccoli, G. & Labib, K. Cdc48 and a ubiquitin ligase drive disassembly of the CMG helicase at the end of DNA replication. *Science* **346**, 1253596 (2014).
11. Moreno, S.P., Bailey, R., Campion, N., Herron, S. & Gambus, A. Polyubiquitylation drives replisome disassembly at the termination of DNA replication. *Science* **346**, 477-481 (2014).
12. Maculins, T., Nkosi, P.J., Nishikawa, H. & Labib, K. Tethering of SCF(Dia2) to the Replisome Promotes Efficient Ubiquitylation and Disassembly of the CMG Helicase. *Curr Biol* **25**, 2254-2259 (2015).
13. Morohashi, H., Maculins, T. & Labib, K. The amino-terminal TPR domain of Dia2 tethers SCF(Dia2) to the replisome progression complex. *Curr Biol* **19**, 1943-1949 (2009).
14. Soucy, T.A. *et al.* An inhibitor of NEDD8-activating enzyme as a new approach to treat cancer. *Nature* **458**, 732-736 (2009).

15. Duda, D.M. *et al.* Structural insights into NEDD8 activation of cullin-RING ligases: conformational control of conjugation. *Cell* **134**, 995-1006 (2008).
16. Saha, A. & Deshaies, R.J. Multimodal activation of the ubiquitin ligase SCF by Nedd8 conjugation. *Molecular cell* **32**, 21-31 (2008).
17. Sonneville, R., Querenet, M., Craig, A., Gartner, A. & Blow, J.J. The dynamics of replication licensing in live Caenorhabditis elegans embryos. *J Cell Biol* **196**, 233-246 (2012).
18. Sonneville, R., Craig, G., Labib, K., Gartner, A. & Blow, J.J. Both Chromosome Decondensation and Condensation Are Dependent on DNA Replication in C. elegans Embryos. *Cell Rep* **12**, 405-417 (2015).
19. Avci, D. & Lemberg, M.K. Clipping or Extracting: Two Ways to Membrane Protein Degradation. *Trends Cell Biol* **25**, 611-622 (2015).
20. Franz, A., Ackermann, L. & Hoppe, T. Ring of Change: CDC48/p97 Drives Protein Dynamics at Chromatin. *Front Genet* **7**, 73 (2016).
21. Ramadan, K., Halder, S., Wiseman, K. & Vaz, B. Strategic role of the ubiquitin-dependent segregase p97 (VCP or Cdc48) in DNA replication. *Chromosoma* (2016).
22. Meyer, H.H., Shorter, J.G., Seemann, J., Pappin, D. & Warren, G. A complex of mammalian ufd1 and npl4 links the AAA-ATPase, p97, to ubiquitin and nuclear transport pathways. *The EMBO journal* **19**, 2181-2192 (2000).

23. Mouysset, J., Kahler, C. & Hoppe, T. A conserved role of Caenorhabditis elegans CDC-48 in ER-associated protein degradation. *Journal of structural biology* **156**, 41-49 (2006).
24. Sarikas, A., Hartmann, T. & Pan, Z.Q. The cullin protein family. *Genome Biol* **12**, 220 (2011).
25. Kloppsteck, P., Ewens, C.A., Forster, A., Zhang, X. & Freemont, P.S. Regulation of p97 in the ubiquitin-proteasome system by the UBX protein-family. *Biochim Biophys Acta* **1823**, 125-129 (2012).
26. Meyer, H., Bug, M. & Bremer, S. Emerging functions of the VCP/p97 AAA-ATPase in the ubiquitin system. *Nat Cell Biol* **14**, 117-123 (2012).
27. Vaz, B., Halder, S. & Ramadan, K. Role of p97/VCP (Cdc48) in genome stability. *Front Genet* **4**, 60 (2013).
28. Pelisch, F. *et al.* Dynamic SUMO modification regulates mitotic chromosome assembly and cell cycle progression in Caenorhabditis elegans. *Nature communications* **5**, 5485 (2014).
29. Merlet, J. *et al.* The CRL2LRR-1 ubiquitin ligase regulates cell cycle progression during C. elegans development. *Development* **137**, 3857-3866 (2010).
30. Starostina, N.G., Simpliciano, J.M., McGuirk, M.A. & Kipreos, E.T. CRL2(LRR-1) targets a CDK inhibitor for cell cycle control in C. elegans and actin-based motility regulation in human cells. *Developmental cell* **19**, 753-764 (2010).

31. Fullbright, G., Rycenga, H.B., Gruber, J.D. & Long, D.T. p97 Promotes a Conserved Mechanism of Helicase Unloading during DNA Cross-Link Repair. *Mol Cell Biol* **36**, 2983-2994 (2016).
32. Semlow, D.R., Zhang, J., Budzowska, M., Drohat, A.C. & Walter, J.C. Replication-Dependent Unhooking of DNA Interstrand Cross-Links by the NEIL3 Glycosylase. *Cell* **167**, 498-511 e414 (2016).
33. Cuvier, O., Stanojcic, S., Lemaitre, J.M. & Mechali, M. A topoisomerase II-dependent mechanism for resetting replicons at the S-M-phase transition. *Genes & development* **22**, 860-865 (2008).
34. Bandau, S., Knebel, A., Gage, Z.O., Wood, N.T. & Alexandru, G. UBXN7 docks on neddylated cullin complexes using its UIM motif and causes HIF1alpha accumulation. *BMC Biol* **10**, 36 (2012).
35. Ossareh-Nazari, B., Katsiarimpa, A., Merlet, J. & Pintard, L. RNAi-Based Suppressor Screens Reveal Genetic Interactions Between the CRL2LRR-1 E3-Ligase and the DNA Replication Machinery in Caenorhabditis elegans. *G3 (Bethesda)* (2016).
36. Dewar, J.M., Low, E., Mann, M., Raschle, M. & Walter, J.C. CRL2Lrr1 promotes unloading of the vertebrate replisome from chromatin during replication termination. *Genes Dev.* **doi:10.1101/gad.291799.116** (2017).
37. Franz, A. *et al.* CDC-48/p97 coordinates CDT-1 degradation with GINS chromatin dissociation to ensure faithful DNA replication. *Mol Cell* **44**, 85-96 (2011).

38. Franz, A. *et al.* Chromatin-associated degradation is defined by UBXN-3/FAF1 to safeguard DNA replication fork progression. *Nature communications* **7**, 10612 (2016).
39. Lee, J.J. *et al.* Complex of Fas-associated factor 1 (FAF1) with valosin-containing protein (VCP)-Npl4-Ufd1 and polyubiquitinated proteins promotes endoplasmic reticulum-associated degradation (ERAD). *J Biol Chem* **288**, 6998-7011 (2013).
40. Menges, C.W., Altomare, D.A. & Testa, J.R. FAS-associated factor 1 (FAF1): diverse functions and implications for oncogenesis. *Cell Cycle* **8**, 2528-2534 (2009).
41. Sharrock, W.J., Sutherlin, M.E., Leske, K., Cheng, T.K. & Kim, T.Y. Two distinct yolk lipoprotein complexes from Caenorhabditis elegans. *J Biol Chem* **265**, 14422-14431 (1990).
42. Gambus, A. *et al.* A key role for Ctf4 in coupling the MCM2-7 helicase to DNA polymerase alpha within the eukaryotic replisome. *EMBO J* **28**, 2992-3004 (2009).
43. Sengupta, S., van Deursen, F., de Piccoli, G. & Labib, K. Dpb2 integrates the leading-strand DNA polymerase into the eukaryotic replisome. *Current biology : CB* **23**, 543-552 (2013).

Figure legends

Figure 1

The CDC-48 co-factor NPL-4 is required for CMG helicase disassembly during S-phase in the *C. elegans* early embryo. (**a**) Illustration of a live-embryo assay for CMG helicase disassembly, comparing control embryos ('normal CMG disassembly') with mutant embryos ('defective CMG disassembly'). Note that the two nuclei derived from oogenesis and spermatogenesis – referred to in this manuscript as the female and male pronuclei - move together during prophase of the first cell cycle. Following nuclear envelope breakdown, the 'male' and 'female' sets of chromosomes then intermingle during metaphase. (**b**) Timelapse video microscopy of the first cell cycle in embryos expressing GFP-SLD-5 and mCherry-HistoneH2B, either untreated or exposed to *npl-4* RNAi. The female pronucleus is shown during S-phase, before convergence with the male pronucleus. Prophase begins during migration of the pronuclei. The arrows indicate examples of persistence of GFP-SLD-5 on chromatin during prophase after depletion of NPL-4. (**c**) Equivalent analysis for embryos expressing GFP-CDC-45. (**d**) Equivalent data for embryos expressing GFP-MCM-3. The arrow indicates the small pool of GFP-MCM-3 that remains on chromatin during early metaphase after depletion of NPL-4. (**e**) Homozygous *GFP-psf-1 / GFP-psf-1* worms were exposed to *npl-4* RNAi or left untreated. Embryos were then isolated and used to generate whole-embryo extracts, before immunoprecipitation of GFP-PSF-1. The indicated proteins were monitored by immunoblotting. (**f**) The same samples were separated in a 4-12% gradient gel, before immunoblotting

with an antibody to poly-ubiquitin chains. (**g**) Equivalent *npl-4* RNAi experiment comparing control worms with homozygous *mcm7-5FLAG-9His* embryos generated by CRISPR-Cas9. The samples were separated in a 3-8% gradient gel, before immunoblotting with antibody to poly-ubiquitin chains. (**h**) Timelapse video microscopy of an *npl-4* RNAi embryo expressing GFP-CDC-45 and mCherry-HistoneH2B. The GFP signal in the female pronucleus was photo-bleached during early S-phase and then monitored in the subsequent mitosis. Lack of recovery of the GFP signal on 'female' chromosomes, compared to the unbleached control male pronucleus, indicated that GFP-CDC45 persists on chromatin after S-phase rather than being reloaded, in embryos lacking NPL-4. The scale bars correspond to 5μm. Unprocessed scans of key immunoblots are shown in Supplementary Figure 8.

Figure 2

CUL-2^{LRR-1} is required for CMG helicase disassembly during S-phase in *C. elegans*. (**a-b**) Embryos from *GFP-sld-5 mCherry-H2B* worms were exposed to the indicated RNAi and processed as in Figure 1b. Timelapse images are shown from S-phase to mid-prophase. Five embryos were examined for each treatment and all behaved equivalently. Arrows denote examples of persistence of GFP-SLD-5 on prophase chromatin and scale bars correspond to 5μm. (**c-d**) Embryos from homozygous *GFP-psf-1 / GFP-psf-1* worms were exposed to the indicated RNAi and processed as in Figure 1e-f. Unprocessed scans of key immunoblots are shown in Supplementary Figure 8.

Figure 3

A mitotic pathway for CMG helicase disassembly is revealed in the absence of CUL-2^{LRR-1}. (**a**) Embryos from *GFP-psf-1 mCherry-H2B* worms were exposed to the indicated RNAi treatments, or empty vector in the control, and then processed as in Figure 1b, except that the figure depicts data from the second embryonic cell cycle (P1 cell). Timelapse images are shown from S-phase to metaphase. GFP-PSF1 initially persists on prophase chromatin following depletion of LRR-1 (the arrows denote examples), before being released in late prophase (indicated by asterisk). Scale bars correspond to 5μm. (**b**) The duration of the indicated cell cycle phases for the experiment in (a) were measured as described in Methods. The data are expressed relative to the length of the corresponding period in control embryos, and represent the mean values (n = 5 embryos; the lines on the boundary of each cell cycle phase indicate standard deviations from the mean). (**c**) Worms homozygous for *GFP-psf-1* and *lrr-1Δ* were grown in parallel to the equivalent heterozygote (control), as described in Methods. After exposure to *atl-1* RNAi (this allows homozygous *lrr-1Δ* germ cells to proceed with meiosis), the resultant embryos were processed as above. The images depict the second embryonic cell cycle (P1 cell), showing persistent association of GFP-PSF-1 with chromatin during prophase (arrows), before release in late prophase (asterisk). (**d-e**) Homozygous *GFP-psf-1* worms were exposed to the indicated RNAi. Embryos were then isolated and processed as in Figure 1e-f. Unprocessed scans of key immunoblots are shown in Supplementary Figure 8.

Figure 4

The mitotic CMG helicase disassembly pathway requires UBXN-3 and is modulated by the SUMO protease ULP-4, both of which become essential when LRR-1 is depleted. (**a**) Embryos from *GFP-psf-1 mCherry-H2B* worms were exposed to the indicated RNAi and processed as in Figure 3a. The arrows indicate persistent association of GFP-PSF1 with mitotic chromatin (throughout mitosis in the case of RNAi to *npl-4*, or after simultaneous RNAi to *lrr-1 + ubxn-3*), whereas the asterisk denotes release of GFP-PSF-1 from chromatin in late prophase in embryos treated only with *lrr-1* RNAi. The scale bars correspond to 5*μ*m. (**b**) Homozygous *GFP-psf-1* worms were exposed to the indicated RNAi and isolated embryos were then processed as in Figure 1e. (**c**) Embryos from *GFP-cdc-45 mCherry-H2B* worms were exposed to the indicated RNAi and processed as above. The data correspond to the AB cell in the second cell cycle, in which *lrr-1 ulp-4* double RNAi leads to persistence of GFP-CDC-45 until at or after nuclear envelope breakdown (8 of 9 embryos tested). (**d**) Worms were fed on plates where the indicated proportion of bacteria expressed *lrr-1* double-stranded RNAi, and embryonic viability was measured as described in Methods (for each timepoint, 69-94 embryos were examined from five adult worms). (**e**) Worms were fed on the indicated proportion of bacteria expressing *ubxn-3* RNAi, either alone or in combination with 10% bacteria expressing *lrr-1* RNAi. The data represent the mean values (n = 3 independent experiments; for each timepoint, 70-100 embryos were examined from five adult worms), with the indicated standard deviations from

the mean value. (**f**) Similar experiment involving increasing doses of *ulp-4* RNAi, with or without 10% *lrr-1* RNAi (n = 3 independent experiments; for each timepoint, 70-100 embryos were examined from five adult worms). Unprocessed scans of key immunoblots are shown in Supplementary Figure 8.

Figure 5

Isolation of the post-termination worm replisome. (**a**) Control or homozygous *GFP-psf-1* worms were exposed to *npl-4* RNAi before being processed as described above for Figure 4. The purified samples were monitored by SDS-PAGE and immunoblotting of the indicated components of the CMG helicase. (**b**) The remainder of the samples were then resolved in a 4-12% gradient gel, which was stained with colloidal coomassie. The major contaminants in both samples (marked with asterisks) represent the four major yolk proteins of the worm early embryo[41]. Each lane was cut into 40 bands as indicated, before analysis of protein content by mass spectrometry (see Supplementary Table 2). (**c**) Comparison of the replisome isolated from active replication forks in budding yeast [1, 42, 43], with the isolated post-termination replisome from worm and frog (this study). For simplicity, some of the proteins that act at forks, but that are not present in the isolated replisome, have been omitted. In addition, Mcm10 has been excluded, since its status at forks and its association with the isolated replisome remain unclear (absent from isolated yeast and worm replisomes under physiological conditions, but co-purifying with frog MCM-3 from digested chromatin post-termination). (**d**) Comparison of isolated

replisome material for the experiment in Supplementary Table 3 (worms treated with *npl-4* RNAi or *npl-4 lrr-1* double RNAi). Unprocessed scans of key immunoblots are shown in Supplementary Figure 8.

Figure 6

$CUL2^{LRR1}$ associates with the post-termination vertebrate replisome and is recruited to chromatin during DNA replication termination in *Xenopus* egg extracts. (**a**) Experimental scheme for isolation of proteins associated with the CMG helicase after termination in the absence of replisome disassembly, in extracts of *Xenopus laevis* eggs. (**b**) Immunoblots of input and the indicated IP samples for the experiment in (a). (**c**) Replisome disassembly was inhibited with the p97 inhibitor NMS873, and LRR1 was then isolated from digested chromatin at the 70' timepoint, in parallel with a control IP with IgG, before detection of the indicated proteins by immunoblotting. (**d**) Chromatin association of the indicated factors was monitored by immunoblotting, at the indicated timepoints after addition of sperm chromatin to egg extracts (except for the -DNA sample that lacked chromatin). Where indicated, replication initiation was blocked by addition of p27(KIP1) or Geminin. The neddylase inhibitor MLN4924 was added to all samples to block replisome disassembly. (**e**) Timecourse experiment comparing chromatin-bound factors in the absence or presence of the neddylation inhibitor MLN4924. (**f**) Replication kinetics were monitored for the experiment in (e), by incorporation of radiolabelled α-dATP into newly synthesised DNA (see also Supplementary Figure 5b; source data for repeats of this experiment are included in

Supplementary Table 6). (**g**) Inhibition of DNA synthesis blocks association of $CUL2^{LRR1}$ with chromatin. DNA synthesis was inhibited with the DNA polymerase inhibitor aphidicolin. Caffeine was added to inactivate the S-phase checkpoint, which otherwise would have reduced the level of CMG on chromatin +Aphidicolin. (**h**) Analogous experiment to that in (e), showing that CUL2-LRR1 accumulated on chromatin with CMG when replisome disassembly was blocked by the p97 inhibitor NMS873, but chromatin recruitment of CUL2-LRR1 was inhibited if DNA replication termination was delayed by addition of the TOPO2 inhibitor ICRF193. Unprocessed scans of key immunoblots are shown in Supplementary Figure 8.

Figure 7

Active $CUL2^{LRR1}$ is required for extraction of CMG components from chromatin during DNA replication termination in *Xenopus* egg extracts. (**a**) Experimental scheme. (**b**) Replication reactions were performed in the presence of MLN4924 to stabilise $CUL2^{LRR1}$ on chromatin during DNA replication termination in mock-depleted extracts (treated with two rounds of IgG-beads). In contrast, neither CUL2 nor LRR1 were detected on chromatin in CUL2-depleted extracts, confirming the efficiency of the depletion. (**c**) Depletion of CUL2 also removes LRR1 from the extract (the panel shows immunoblots of the antibody-coupled beads after each of the two rounds of depletion). (**d**) Kinetics of DNA synthesis in extracts subjected to two rounds of immunoprecipitation with control IgG ('mock depletion') or with antibodies to Hs_CUL2-RBX1 ('CUL2 depletion', see Methods). Source data for repeats of

this experiment are included in Supplementary Table 6. (**e**) In an analogous experiment, replication reactions were performed in 'mock-depleted' and CUL-depleted extracts. A pulse of α-dATP was added for 3' at either the 60' or 120' timepoints, and the incorporation of radiolabel into nascent DNA was monitored after isolation of total DNA, indicating that replication proceeded and completed with similar kinetics in both extracts, consistent with the data in (d). (**f**) Kinetics of chromatin association of the indicated factors for the same experiment shown in (a-b). Note that the MCM7 immunoblot is over-exposed in order to reveal the ubiquitylated forms of the protein. (**g**) Mock-depleted or CUL2-depleted extracts were supplemented with the indicated recombinant proteins (X.l. LRR1, wt/mutant Hs_CUL2-RBX1 – see Methods), and chromatin was isolated from the 120' timepoint in a similar experiment to that described above. Unprocessed scans of key immunoblots are shown in Supplementary Figure 8.

Competing Financial Interests

The authors confirm that they have no competing financial interests.

Legends to Supplementary Information

Supplementary Figure 1

The CDC-48_UFD-1_NPL-4 complex is required for CMG helicase disassembly in *C. elegans*. (**a**) *cdc-48* RNAi leads to persistence of GINS and CDC-45 on chromatin during prophase and throughout mitosis (examples indicated by arrows). (**b**) Adaptors of CDC-48 in *C. elegans*. (**c**) *ufd-1* RNAi leads to persistence of GINS and CDC-45 on chromatin during prophase and throughout mitosis (examples indicated by arrows). (**d**) Equivalent experiment to that in Figure 1d, illustrating the effect of *npl-4* RNAi on embryos expressing GFP-MCM-3. To help visualise the small proportion of GFP-MCM-3 on chromatin in early metaphase (marked by an arrow), the experiment also included RNAi to the 3'UTR of endogenous MCM3 (this 3' UTR is not present in the GFP-MCM-3 transgene), to increase the incorporation of GFP-MCM3 into replication complexes. (**e**) *cdc-48* RNAi experiment, analogous to that in Figure 1d. (**f**) Homozygous *GFP-psf-1* worms were exposed to the indicated RNAi. Embryos were then isolated and processed as in Figure 1e-f. The middle panels show that the amount of CMG isolated from RNR-1 depleted extract was reduced compared to control (compare levels of MCM-7, MCM-2 and CDC-45), due to the inhibition of DNA replication in each embryonic cell cycle. In the right panels, loading of the GFP-PSF-1 IP samples was adjusted to obtain a similar level of CMG (compare MCM-2 and CDC-45). (**g**-**h**) Photobleaching experiments for GFP-SLD5 and GFP-MCM3, equivalent to the experiment in Figure 1h. The scale bars correspond to 5μm. Unprocessed scans of key immunoblots are shown in Supplementary Figure 8.

Supplementary Figure 2

CUL-2^{LRR-1} is required for removal of GINS from chromatin during S-phase in *C. elegans*. (**a**) *C. elegans* contain six families of cullin complexes, each with a specific cullin and a unique set of substrate adaptors. (**b**) Embryos from *GFP-sld-5 mCherry-H2B* worms were exposed to RNAi against the indicated cullins and processed as in Figure 2. Timelapse images are shown from S-phase to mid-prophase. (**c**) Six forms of the CUL-2 ligase in *C. elegans*, each with a unique substrate adaptor. (**d**) Embryos from *GFP-sld-5 mCherry-H2B* worms were exposed to RNAi against the indicated substrate adaptors of CUL-2 and processed as in Figure 2. Timelapse images are shown from S-phase to mid-prophase. RNAi for *zyg-11* produces meiotic defects and leads to abnormal nuclear morphology in the first embryonic cell cycle. Arrows in this figure indicate the persistent association of GFP-SLD-5 with mitotic chromatin in embryos treated with *npl-4* RNAi. Scale bars correspond to 5μm.

Supplementary Figure 3

A new pathway for CMG helicase disassembly acts during mitosis. (**a**) Embryos from *GFP-psf-1 mCherry-H2B* worms were exposed to the indicated RNAi and processed as in Figure 3. Timelapse images of the first embryonic cell cycle are shown from S-phase to metaphase. GFP-PSF1 initially persists on prophase chromatin following RNAi to components of CUL-2^{LRR-1} (the arrows denote examples), before being released in late prophase (indicated by asterisks). (**b**) Extended timecourses for the GFP-SLD-5 data presented in

Figure 2a-b. (**c**) Data from the first cell cycle, for the experiment in Figure 3b. (**d**) Embryos from *GFP-cdc-45 mCherry-H2B* worms were exposed to the indicated RNAi and processed as above. (**e**) Illustration of CMG disassembly defects produced either by depletion of CDC-48 / UFD-1 / NPL-4, or by depletion of components of CUL-2^{LRR-1}. Scale bars correspond to 5μm.

Supplementary Figure 4

The mitotic disassembly pathway for the CMG helicase requires UBXN-3 and is modulated by ULP-4. (**a**) Embryos from *GFP-sld-5 mCherry-H2B* worms were exposed to the indicated RNAi and processed as in Figure 4a. The arrows indicate persistent association of GFP-PSF1 with mitotic chromatin (throughout mitosis in the case of RNAi to *npl-4*, or after simultaneous RNAi to *lrr-1 + ubxn-3*), whereas the asterisk denotes release of GFP-PSF-1 from chromatin in late prophase in embryos treated only with *lrr-1* RNAi. Scale bars correspond to 5μm. (**b**) Embryos from *GFP-cdc-45 mCherry-H2B* worms were processed as for Figure 4b. (**c**) Embryos from *GFP-psf-1 mCherry-H2B* worms were exposed to the indicated RNAi and processed as above. The data correspond to the AB cell in the second cell cycle and CMG components remained on chromatin until at or after nuclear envelope breakdown in 3/5 embryos treated with *lrr-1 ulp-4* double RNAi. The panel shows an example of an embryo where CMG persists on chromatin until nuclear envelope breakdown upon co-depletion of LRR-1 and ULP-4. (**d**) Data from a similar experiment, corresponding to the EMS cell in the third cell cycle. Note that in this case we also depleted the ATL-1 checkpoint kinase, to shorten the

otherwise long cell cycle delay that is induced by the combination of *ulp-4 lrr-1* double RNAi. CMG components remained on chromatin until late metaphase in 5/5 embryos treated with *lrr-1 ulp-4 atl-1* triple RNAi. CMG was extracted normally from chromatin during S-phase in embryos subjected to *ulp-4 atl-1* double RNAi (5/5 embryos tested), whereas *lrr-1 atl-1* double RNAi resembled *lrr-1* single RNAi treatment (CMG extracted before the end of prophase in 5/5 embryos).

Supplementary Figure 5

Additional supplementary material for experiments with *Xenopus* egg extracts. (**a**) In a similar experiment to that in Figure 6c, replisome disassembly was blocked during chromosome replication by addition of MLN4924 to *Xenopus* egg extracts. After isolation of chromatin and digestion of DNA, immunoprecipitation of LRR1 led to co-depletion of CUL2. (**b**) Analysis of ongoing DNA synthesis at the indicated timepoints for the experiment in Figure 6e-f, by addition of short pulses of α-dATP (see Methods). Data for repeats of this experiment are included in Supplementary Table 6. (**c**) Replication kinetics for the experiment in Figure 6h, measured by monitoring total incorporation of α-dATP into nascent DNA by the indicated timepoints (see Methods). Data for repeats of this experiment are included in Supplementary Table 6. Unprocessed scans of key immunoblots from this Figure are shown in Supplementary Figure 8.

Supplementary Figure 6

CUL2 is very highly conserved in vertebrates. Alignment of *Xenopus* CUL2 with the human and mouse orthologues, showing that the mammalian and frog proteins are almost identical. Moreover, previous work indicated that all key residues in CUL2 that contact EloB-C and substrate adaptors are 100% conserved between the human and frog orthologues[1].

Supplementary Figure 7

Validation of new antibodies generated in this study for *C. elegans* proteins. (**a**-**d**) In each case, RNAi was used to deplete the corresponding protein, before immunoblotting of embryonic extracts (upper panels). Ponceau S staining of the nitrocellulose membare (lower panels) provides a loading control in each case.

Supplementary Figure 8

Unprocessed scans of key immunoblots. (**a**) Raw immunoblot data for Figure 1e, with red boxes indicating the crops used to construct Figure 1e. (**b**) Equivalent data for Figure 1f. (**c**) Equivalent data for Figure 1g. (**d**) Equivalent data for Figure 6d. (**e**) Equivalent data for Figure 6h.

Supplementary Table 1

Factors targeted by RNAi in screen for components of the mitotic CMG disassembly pathway.

Supplementary Table 2

CUL-2^{LRR-1} associates with the isolated 'post-termination' replisome from *C. elegans*. Summary of mass spectrometry data for experiment shown in Figure 5b.

Supplementary Table 3

LRR-1 is required for CUL-2 to associate with the 'post-termination' worm replisome. Summary of mass spectrometry data for experiment shown in Supplementary Figure 5d.

Supplementary Table 4

CUL2^{LRR1} associates with the 'post-termination' frog replisome. Summary of mass spectrometry data for experiment summarised in Figure 6a.

Supplementary Table 5

The 'post-termination' replisome associates with purified frog CUL2^{LRR1}. Summary of mass spectrometry data for an equivalent experiment to that shown in Figure 6c.

Supplementary Table 6

Statistics Source Data. Source data of all repeats of the experiments in Figure 6f, Figure 7d, Supplementary Figure 5b and Supplementary Figure 6g.

Supplementary Table 7

Antibody dilutions for immunoblots.

Supplementary Table 8

Sequence of oligonucleotide primers used to generate RNAi vectors for depletion of *C. elegans* proteins.

Supplementary Movie 1

The CMG helicase component PSF-1 does not associate with condensing chromatin during mitotic prophase or throughout mitosis. Video of a single optical section through an embryo expressing GFP-PSF-1 (left panel) and mCherry-Histone H2B (right panel) progressing throughout the first and second embryonic cell cycles. Images were acquired every 10 sec with a spinning disk confocal microscope and processed with ImageJ software. The female and male pronuclei are orientated respectively towards the left and right of the video.

Supplementary Movie 2

GFP-PSF-1 associates with condensing chromatin during prophase in embryos depleted for NPL-4 and remains on chromatin throughout mitosis. Images were acquired and analysed as for Supplementary Movie 1.

Supplementary Movie 3

FRAP analysis of GFP-CDC-45 after depletion of NPL-4. The movie was generated as above and shows an embryo expressing GFP-CDC-45 (left panel) and mCherry-Histone H2B (right panel). The female pronucleus (left

side of the embryo) was photobleached during early S-phase (shown as a white disk in the video at 1'50") and the chromosomes from the female and male pronuclei were then analysed during the following mitosis (see 19'30" to 24'50"). No recovery of the GFP-CDC-45 signal was observed on the female chromatin, indicating that depletion of NPL-4 causes CDC-45 to persist on chromatin from S-phase until the end of mitosis.

Supplementary Movie 4

GFP-PSF-1 associates with condensing chromatin during prophase in embryos depleted for CUL-2, but is then released from chromatin during late prophase. Images were acquired and analysed as for Supplementary Movie 1. Note that depletion of CUL-2 leads to meiotic defects in the embryo and thus to abnormal nuclear morphology, reflecting the important role of CUL-2^{ZYG-11} during the second meiotic cell division [2,3]. In addition, mitotic entry is delayed in the first embryonic cell cycle after depletion of CUL-2.

Supplementary Movie 5

GFP-PSF-1 associates with condensing chromatin during prophase in embryos depleted for LRR-1, but is then released from chromatin during late prophase. Images were acquired and analysed as for Supplementary Movie 1. The association of GFP-PSF-1 with prophase chromatin can be seen in the first embryonic cell cycle (P0 cell) from 3'20" to 5'50" and during the second cell cycle from 24'30" to 26'10" for the AB cell (left side of embryo) or from 27'30" to 29'10" for the P1 cell (right side).

Supplementary Movie 6

GFP-PSF-1 remains on chromatin throughout mitosis in embryos depleted for both UBXN-3 and LRR-1. Images were acquired and analysed as for Supplementary Movie 1.

Supplementary Movie 7

GFP-PSF-1 is released from chromatin before prophase in ubxn-3 RNAi embryos. Images were acquired and analysed as for Supplementary Movie 1.

References

1. Nguyen, H.C., Yang, H., Fribourgh, J.L., Wolfe, L.S. & Xiong, Y. Insights into Cullin-RING E3 ubiquitin ligase recruitment: structure of the VHL-EloBC-Cul2 complex. *Structure* **23**, 441-449 (2015).
2. Liu, J., Vasudevan, S. & Kipreos, E.T. CUL-2 and ZYG-11 promote meiotic anaphase II and the proper placement of the anterior-posterior axis in C. elegans. *Development* **131**, 3513-3525 (2004).
3. Sonneville, R. & Gonczy, P. Zyg-11 and cul-2 regulate progression through meiosis II and polarity establishment in C. elegans. *Development* **131**, 3527-3543 (2004).

Sonneville et al Figure 1

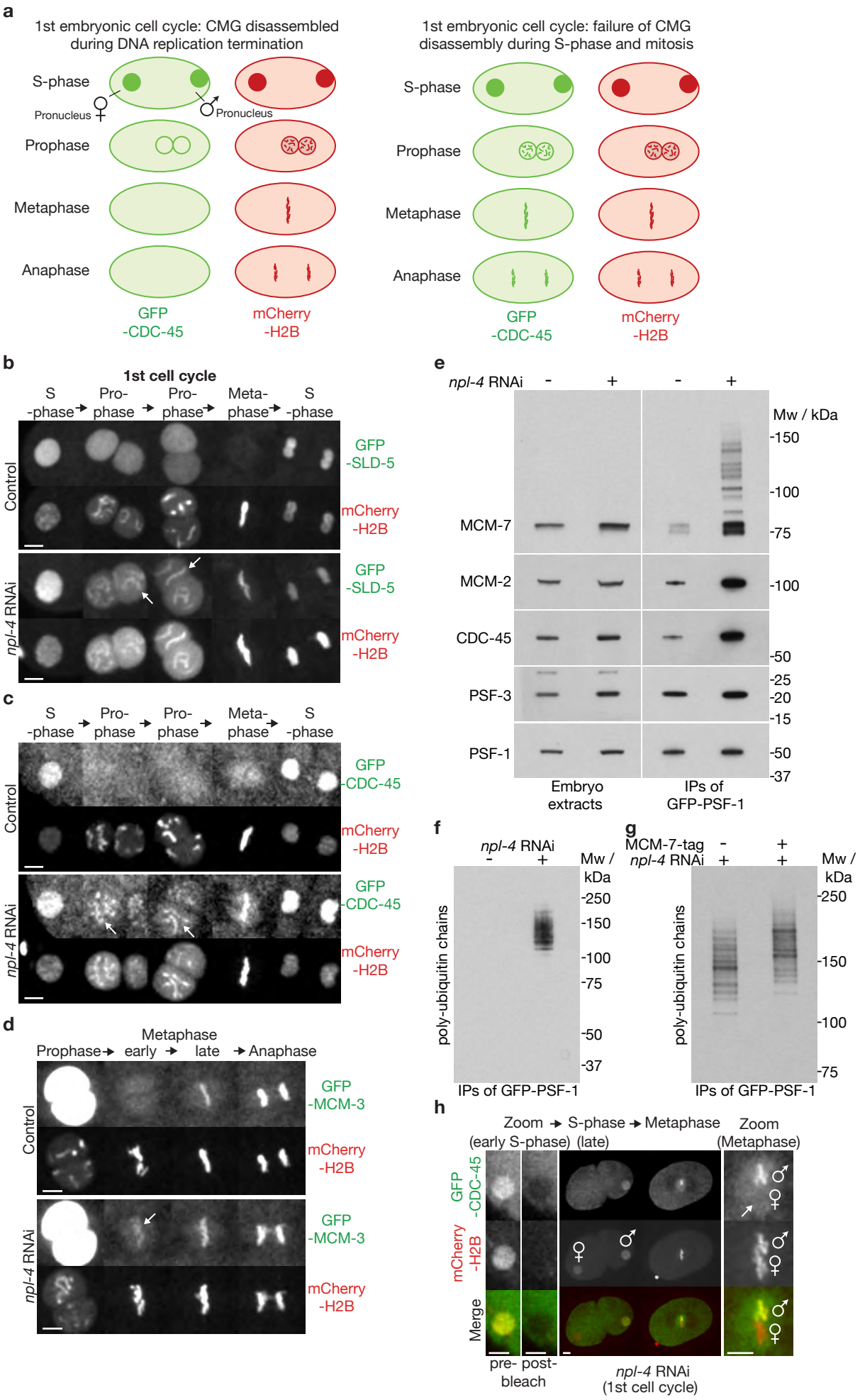

Sonneville et al Figure 2

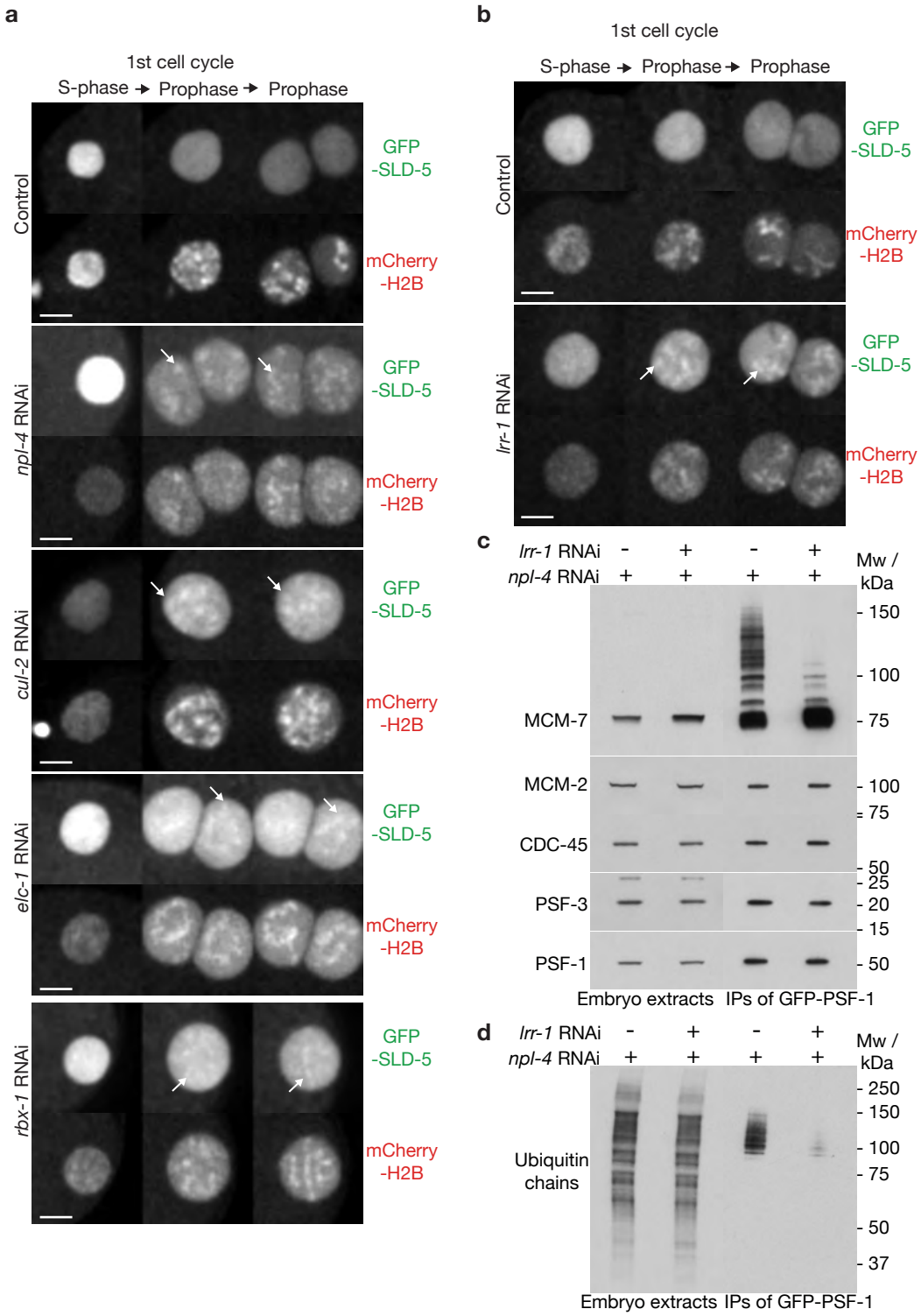

Sonneville et al Figure 3

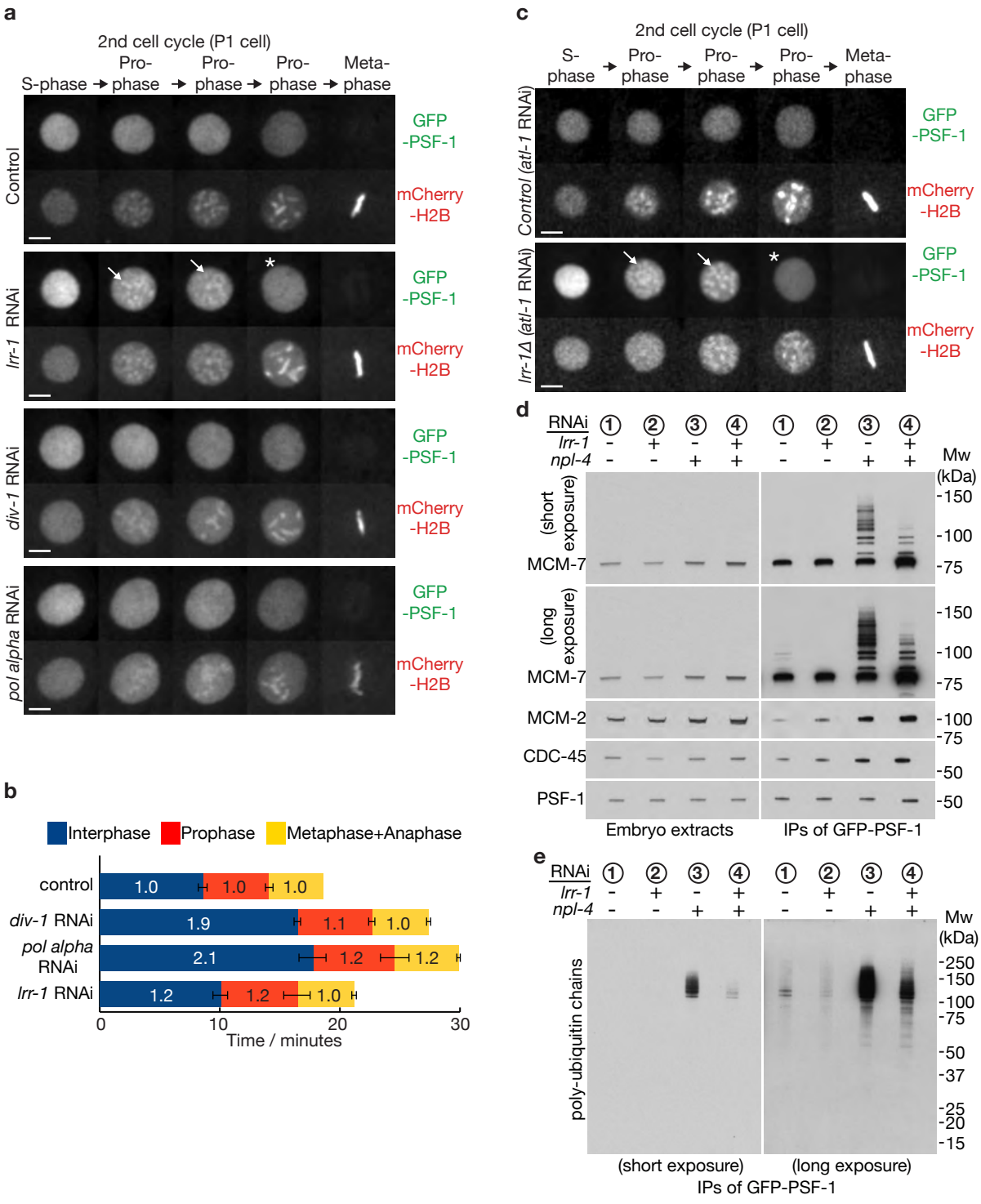

Sonneville et al Figure 4

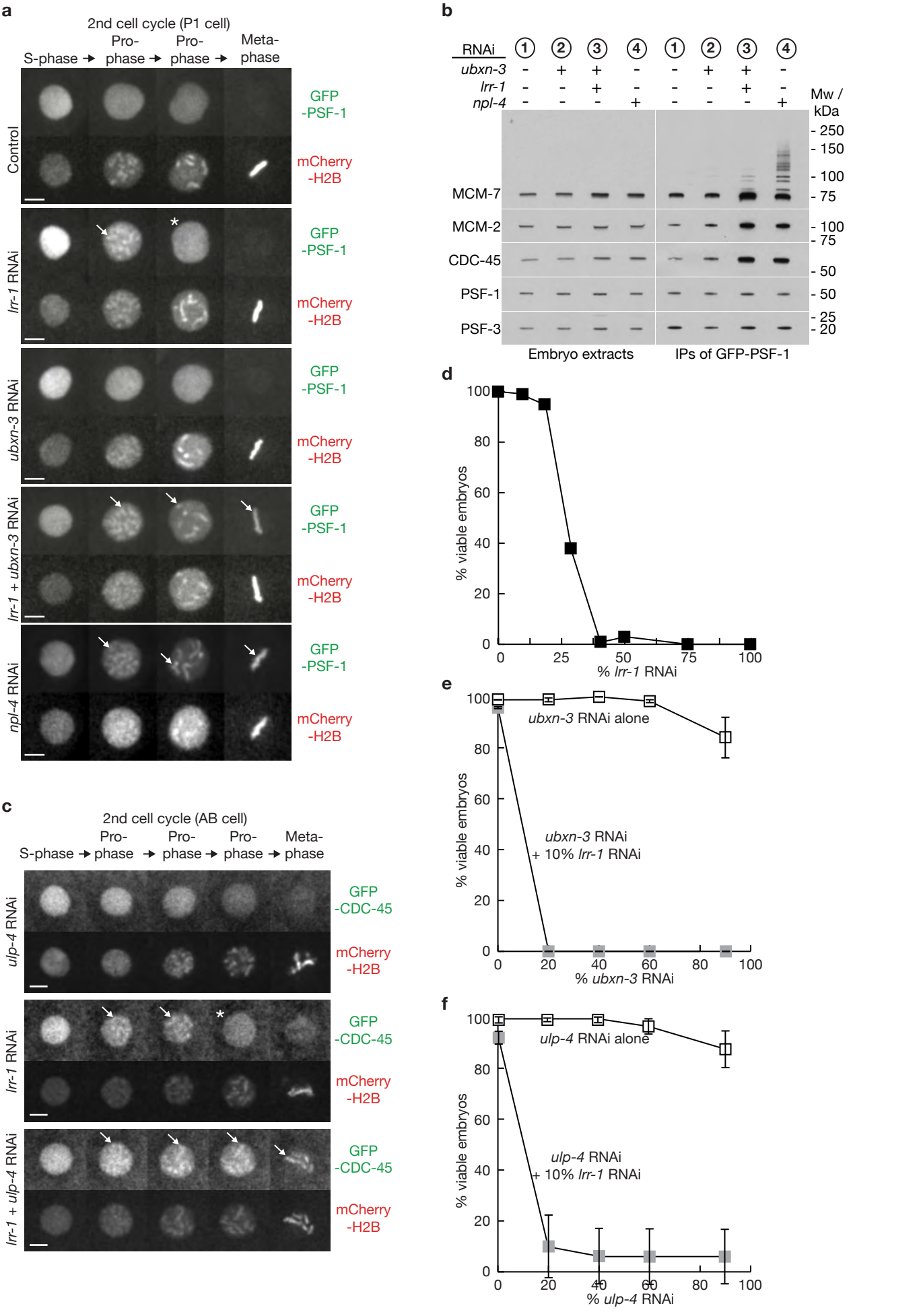

Sonneville et al Figure 5

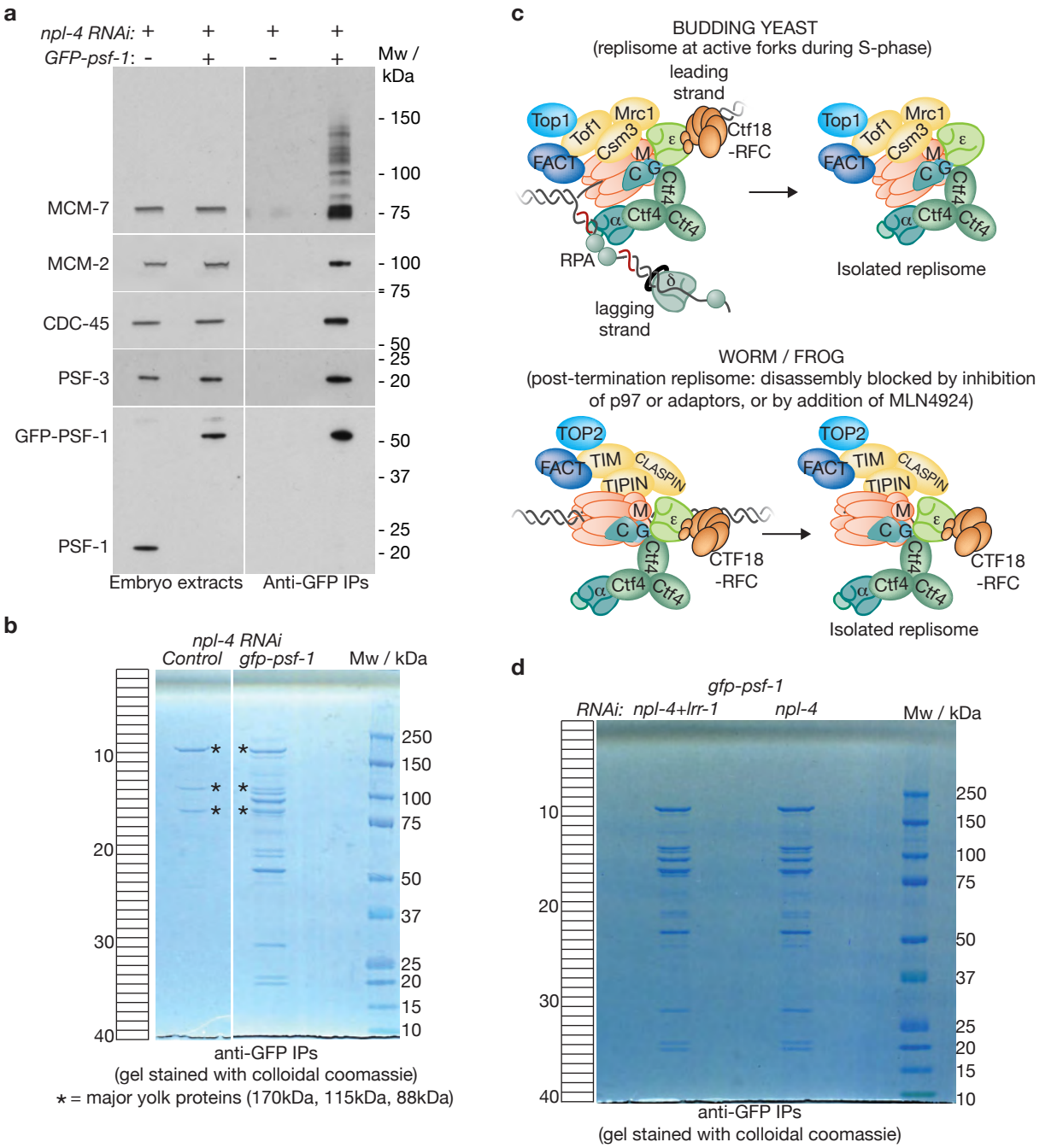

Sonneville et al Figure 6

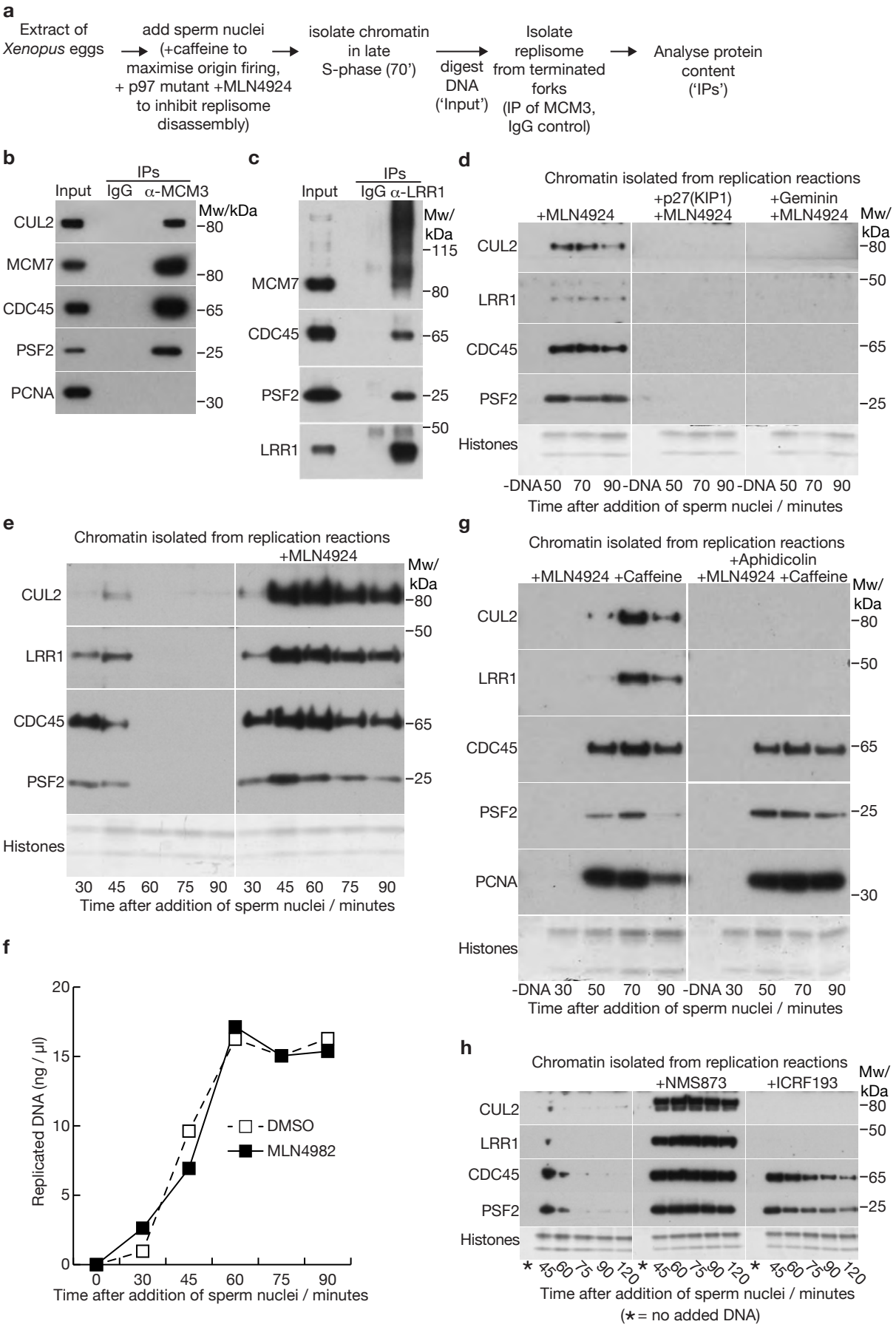

Sonneville et al Figure 7

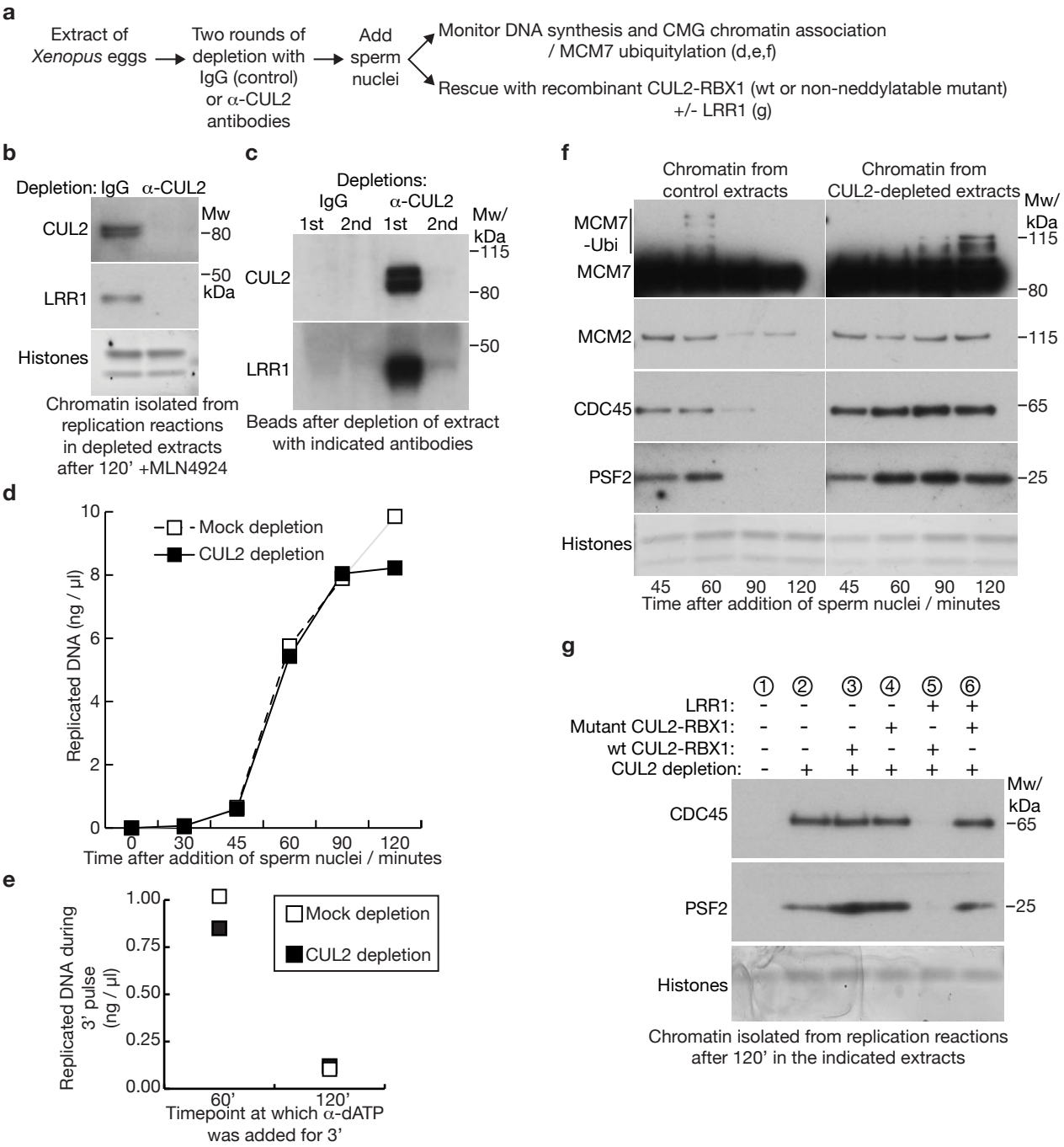

Sonneville et al Supplementary Figure 1

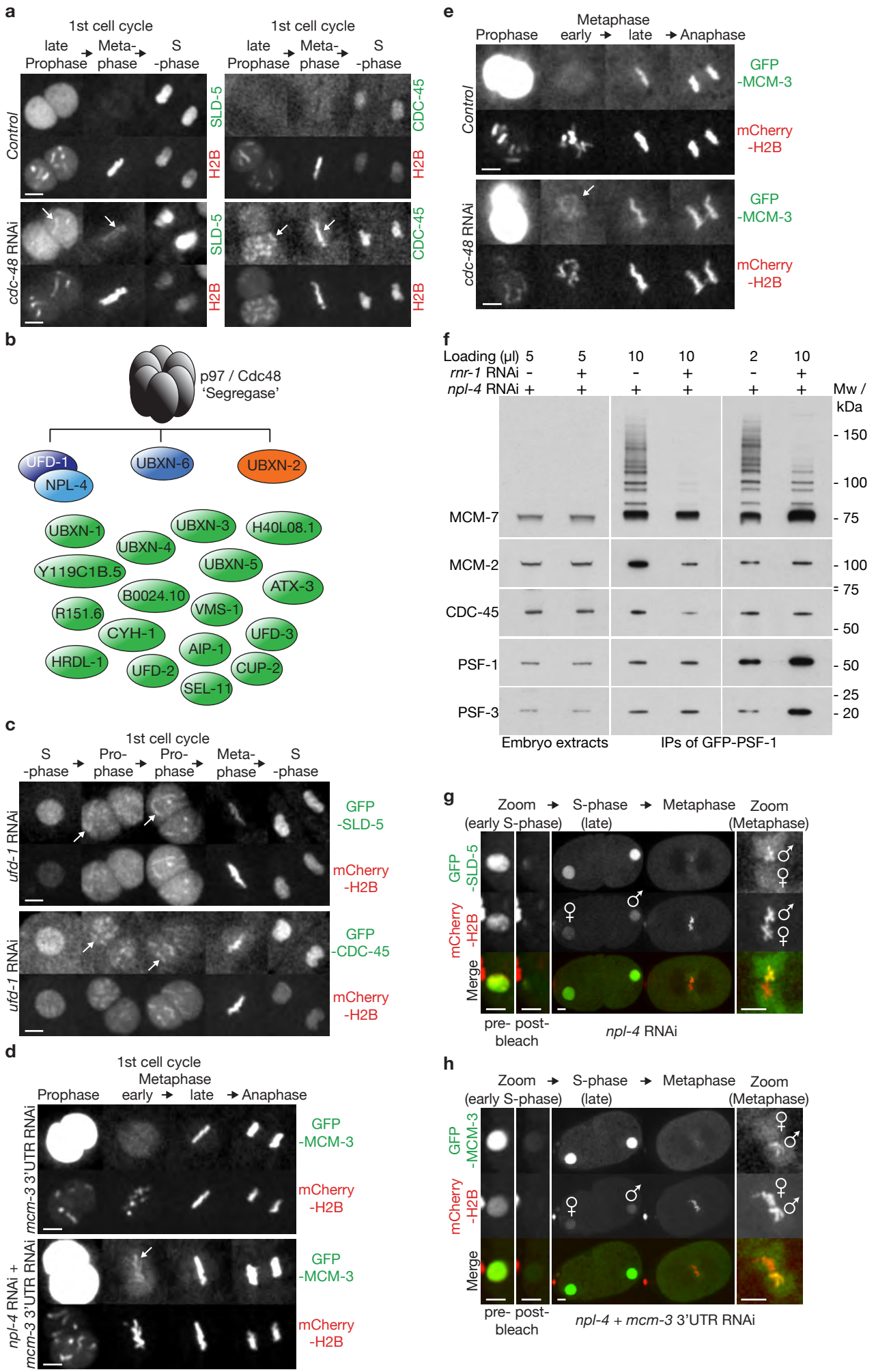

Sonneville et al Supplementary Figure 2

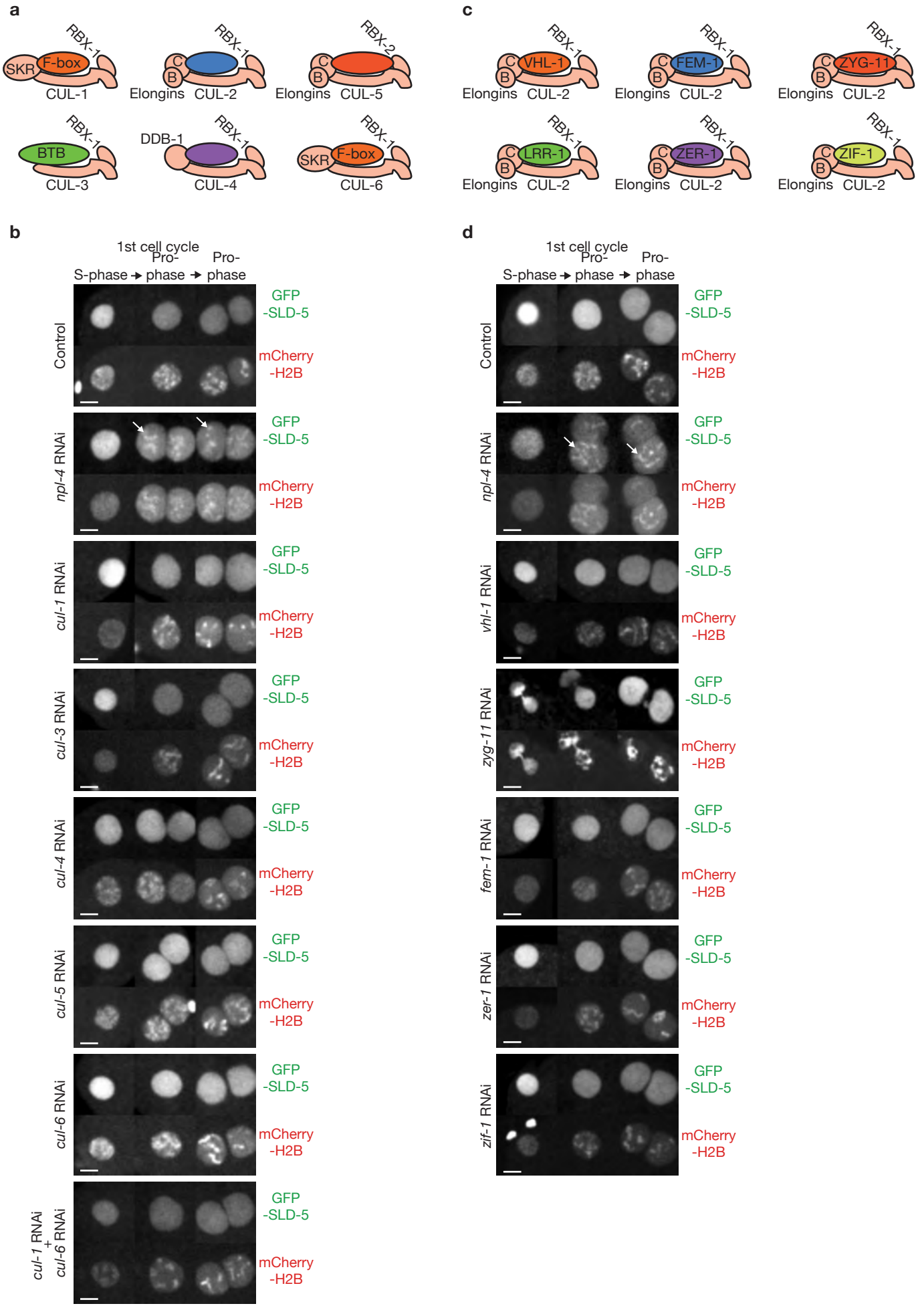

Sonneville et al Supplementary Figure 3

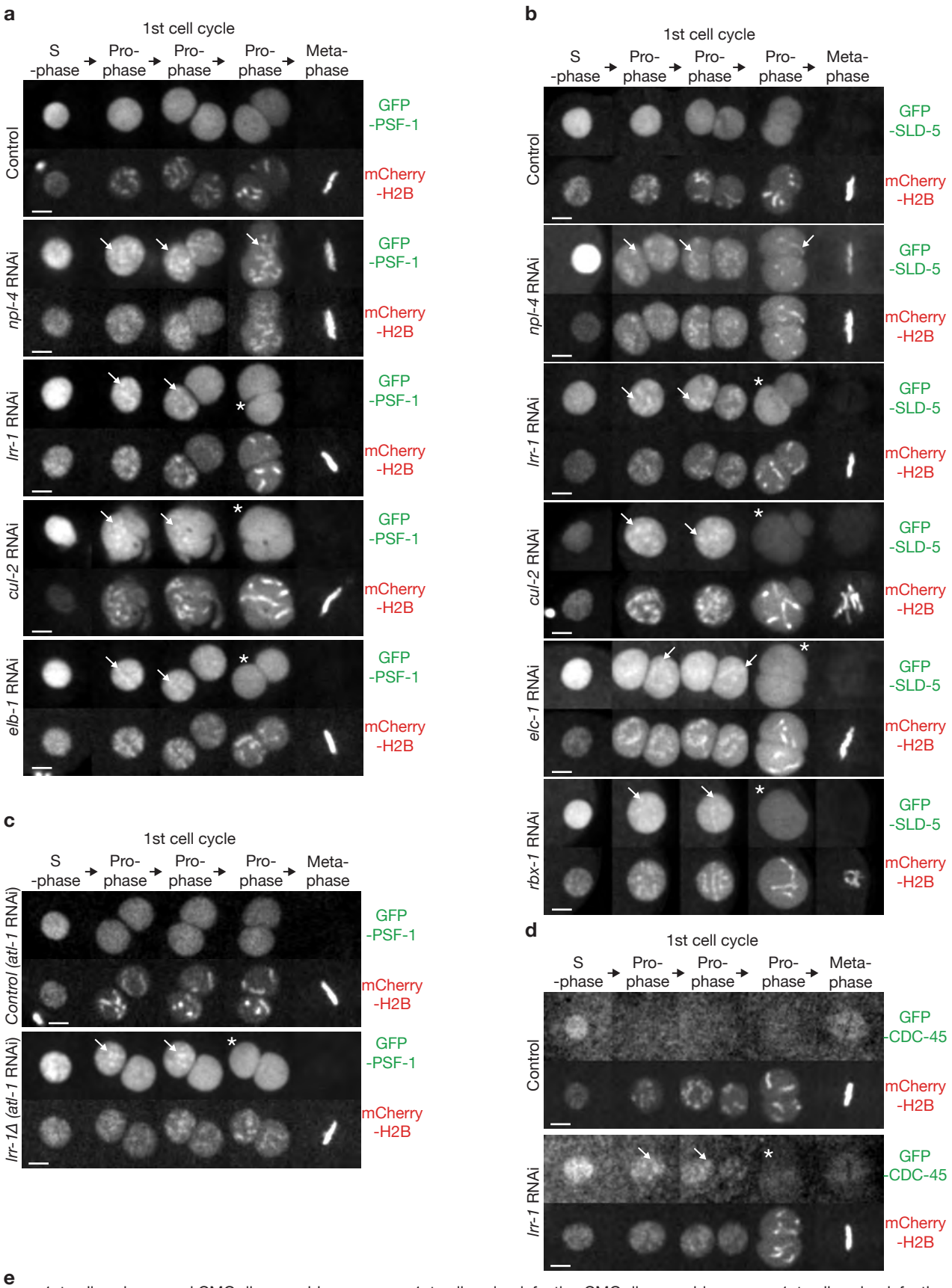

Sonneville et al Supplementary Figure 4

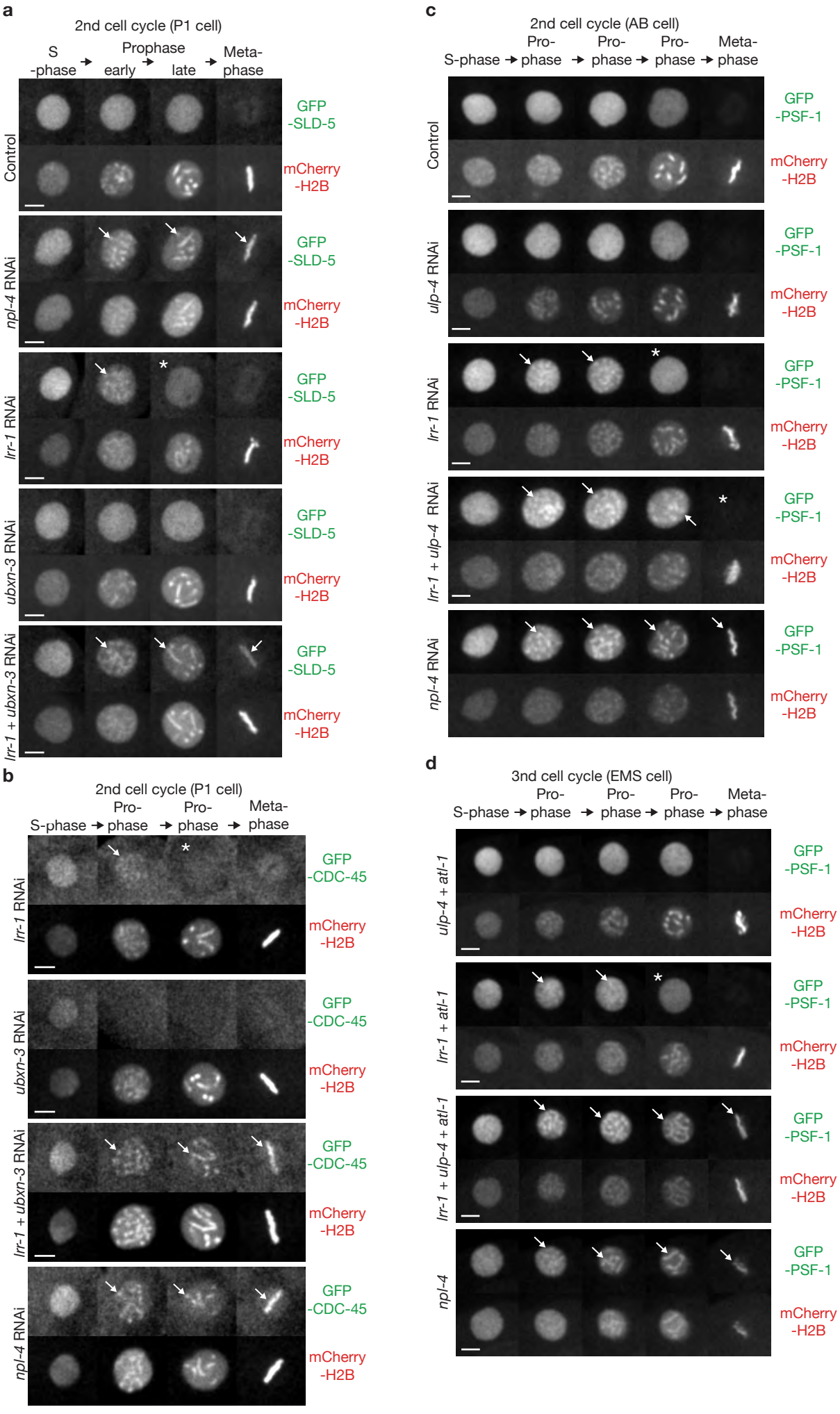

Sonneville et al Supplementary Figure 5

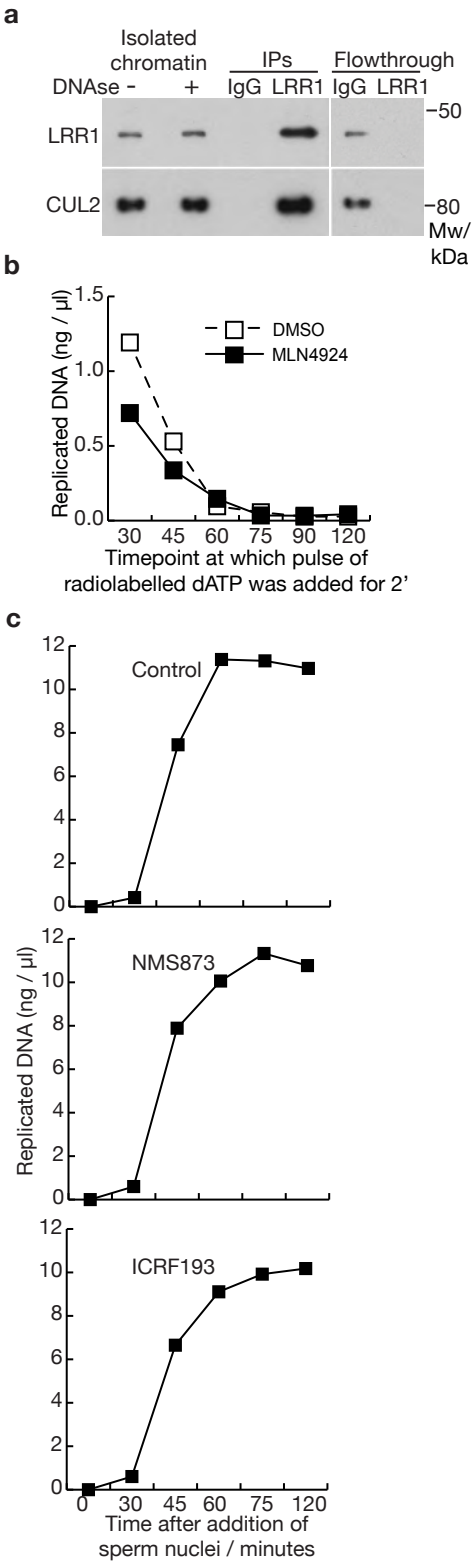

Sonneville et al Supplementary Figure 6

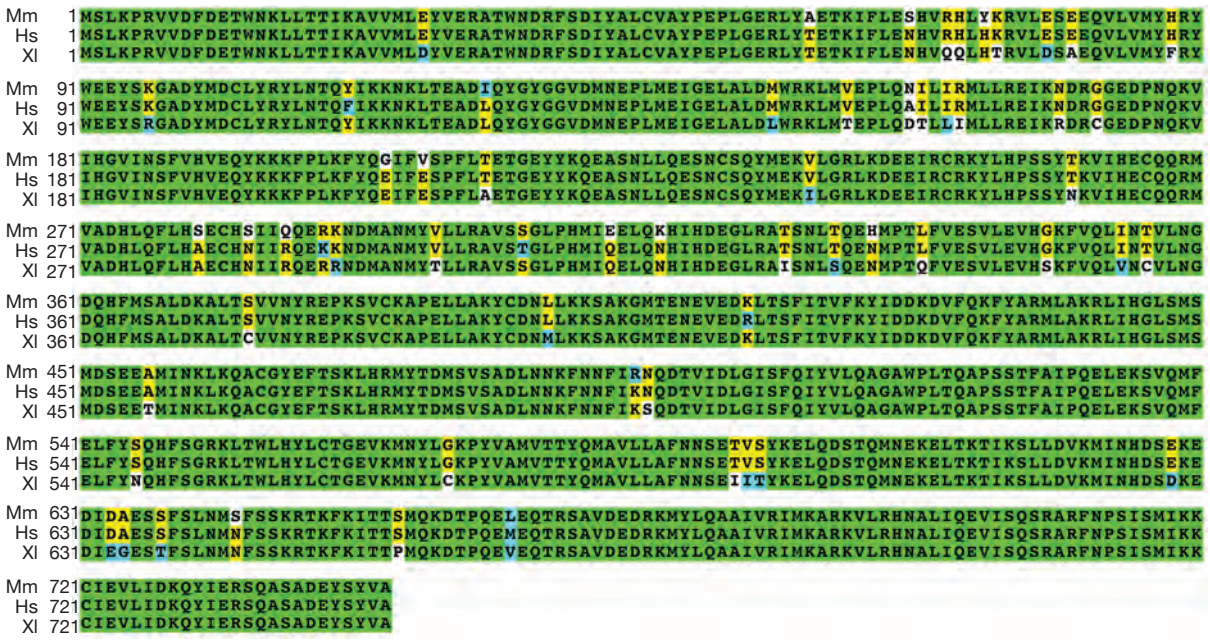

Protein	Properties
AIR-2	Aurora protein kinase
PLK-1	Polo protein kinase
CYB-3	Cyclin B
CYA-1	Cyclin A
GSK-3	GSK3 protein kinase
MBK-2	MBK2 protein kinase
BRC-1	BRCA1 orthologue
BRD-1	BARD1 orthologue
D2085.4	HECT ligase (meiosis)
SMC-5	SMC5-6 complex
NSE-1	SMC5-6 complex
C32D5.10	RING (RNF146 orthologue)
C32D5.11	RING (Pex10 orthologue)
EEL-1	HECT ligase
Y47G6A.31	RING (homology with RNF4)
SPAT-3	RING (H2A ubiquitylation)
MIG-32	RING (H2A ubiquitylation)
RNF-113	RNF113 orthologue
VPS-11	VPS11 orthologue
TO1G5.7	RING (homology with RNF8)
ATL-1	ATR checkpoint protein kinase
ATM-1	ATM checkpoint protein kinase
SMC-4	Condensin
PIF-1	DNA helicase
DVC-1	Spartan protease
SMO-1	SUMO
UBC-9	SUMO E3 enzyme
ULP-4	Major mitotic SUMO protease

Protein	Total spectral counts for control IP (npl-4 RNAi)
MCM-2 (99 kDa)	62
MCM-3 (91 kDa)	167
MCM-4 (92 kDa)	87
MCM-5 (85 kDa)	137
MCM-6 (91 kDa)	70
MCM-7 (82 kDa)	150
CDC-45 (66 kDa)	12
PSF-1 (23 / 54 kDa)	3
PSF-2 (20 kDa)	15
PSF -3 (22 kDa)	2
SLD-5 (26 kDa)	0
CTF-4 (123 kDa)	12
SPT-16 (117 kDa)	14
SSRP-1A/B (79/78 kDa)	0 / 2
CTF-18 (97 kDa)	0
TIM-1 (157 kDa)	0
TIPIN (27 kDa)	0
TOPO-2 (172 kDa)	5
CLASPIN (85 kDa)	0
POLE1 (245 kDa)	37
POLE2 (59 kDa)	8
CUL-2 (98 kDa)	26
LRR-1 (51 kDa)	0

Total spectral counts for PSF-1 IP (npl-4 RNAi)

1244
1110
967
1381
1065
1577
563
1624
335
399
516

94
714
124 / 229
53
624
74
37
51
211
33

156
67

Protein	**Total spectral counts for PSF-1 IP (*npl-4* RNAi)**
MCM-2 (99 kDa)	585
MCM-3 (91 kDa)	655
MCM-4 (92 kDa)	493
MCM-5 (85 kDa)	682
MCM-6 (91 kDa)	483
MCM-7 (82 kDa)	1088
CDC-45 (66 kDa)	219
PSF-1 (23 / 54 kDa)	1033
PSF-2 (20 kDa)	274
PSF -3 (22 kDa)	319
SLD-5 (26 kDa)	338
CTF-4 (123 kDa)	64
SPT-16 (117 kDa)	246
SSRP-1A/B (79/78 kDa)	66 / 111
CTF-18 (97 kDa)	32
TIM-1 (157 kDa)	380
TIPIN (27 kDa)	51
TOPO-2 (172 kDa)	15
CLASPIN (85 kDa)	24
POLE1 (245 kDa)	51
POLE2 (59 kDa)	27
CUL-2 (98 kDa)	95
LRR-1 (51 kDa)	81

Total spectral counts for PSF-1 IP (*lrr-1 npl-4* RNAi)

800
688
552
644
630
827
211
908
217
260
203
73
343
80 / 153
12
319
16
16
20
88
29
20
5

Protein	Total spectral counts for control IP
MCM2 (100 kDa)	17
MCM3 (90 kDa)	17
MCM4 (97 kDa)	7
MCM5 (82 kDa)	30
MCM6 (93 kDa)	39
MCM7 (82 kDa)	24
CDC45 (66 kDa)	2
PSF1 (23 kDa)	0
PSF2 (21 kDa)	0
PSF 3 (24 kDa)	0
SLD5 (26 kDa)	0
CTF4 (125 kDa)	6
SPT16 (118 kDa)	3
SSRP (79 kDa)	0
TIMELESS (149 kDa)	0
TIPIN (40 kDa)	0
TOP2a (179 kDa)	6
CLASPIN (146 kDa)	0
POLA1 (165 kDa)	0
POLA2 (67 kDa)	0
POLE1 (261 kDa)	2
POLE2 (60 kDa)	0
CTF18 (113 kDa)	0
RFC3 (40 kDa)	4
RFC4 (40 kDa)	2
RFC2 (38 kDa)	0
p97 / CDC48 (89 kDa)	0
UFD1 (35 kDa)	0
NPL4 (69 kDa)	0
CUL2 (87 kDa)	0
LRR1 (47 kDa)	0
Elongin B (13 kDa)	0
Elongin C (12 kDa)	0

Total spectral counts for MCM3 IP

975
1111
947
927
888
905
277
62
33
55
44

554
453
229
171
54
484
72
109
7
543
103
172
36
31
27

361
4
19

101
46
5
7

Protein	Total spectral counts for control IP
CUL2 (87 kDa)	14
LRR1 (47 kDa)	8
Elongin B (13 kDa)	0
Elongin C (12 kDa)	0
MCM2 (100 kDa)	47
MCM3 (90 kDa)	47
MCM4 (97 kDa)	30
MCM5 (82 kDa)	46
MCM6 (93 kDa)	68
MCM7 (82 kDa)	50
CDC45 (66 kDa)	14
PSF1 (23 kDa)	2
PSF2 (21 kDa)	0
PSF 3 (24 kDa)	2
SLD5 (26 kDa)	2
CTF4 (125 kDa)	42
SPT16 (118 kDa)	29
SSRP (79 kDa)	6
TIMELESS (149 kDa)	0
TIPIN (40 kDa)	0
TOP2a (179 kDa)	20
CLASPIN (146 kDa)	2
POLA1 (165 kDa)	0
POLA2 (67 kDa)	0
POLE1 (261 kDa)	3
POLE2 (60 kDa)	4
CTF18 (113 kDa)	7
p97 / CDC48 (89 kDa)	0

Total spectral counts for LRR1 IP

748
197
20
26

275
252
190
243
251
216
128
25
17
21
25

350
136
40
62
26
283
107
17
2
145
31
29

16